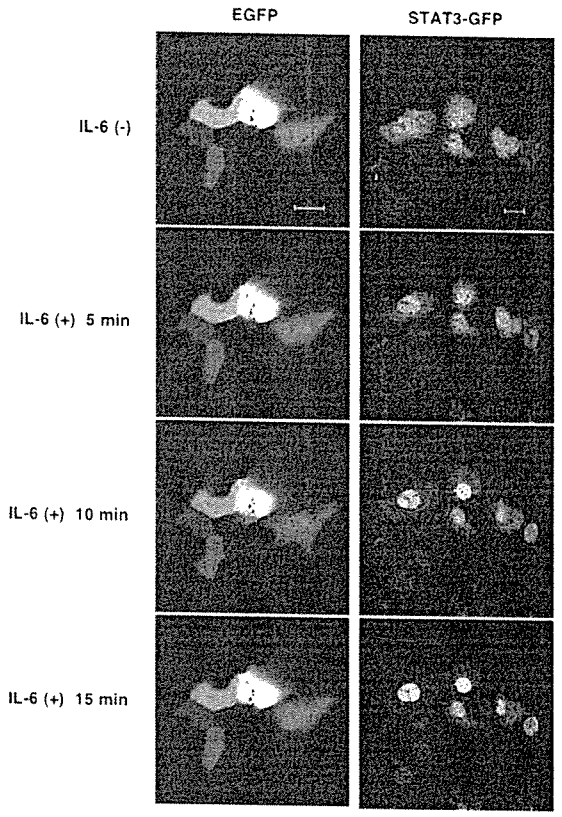

Fig. 1. Translocation of STAT3-GFP from cytoplasm to nucleus by IL-6 stimulation. Hep3B cells were transfected with the expression vector of EGFP or STAT3-GFP and stable transformant clone expressing EGFP (left) or STAT3-GFP (right) was established. Confocal imaging data were obtained using LSM before IL-6 addition and at 5, 10, or 15 min after IL-6 addition. Each scale bar represents the length for 20 μm.

STAT3-GFP from cytoplasm to the nucleus was observed gradually from 5 to 15 min after IL-6 addition (Fig. 1, right panel). These results were consistent with the previous data for translocation of STAT3 by IL-6 stimulation using Western blot analysis [27,28].

FCS measurement of EGFP in living cells and statistical analysis of its diffusion constants

As shown in Fig. 2A, the diffusion state of EGFP was measured at five positions in a single living cell as a control. No difference for the correlation curve was observed by the measurement at these positions after IL-6 addition (Fig. 2B). The diffusion state of EGFP in the living cell did not change by IL-6 addition. It was demonstrated that almost no change for the molecular dynamics of EGFP was induced in Hep3B cells after IL-6 addition.

The distribution of the fraction for each calculated diffusion constant in Hep3B cells was fitted with one ($i = 1$, as shown in the Eq. (1) in Materials and methods), two ($i = 2$), and three diffusion component-models ($i = 3$) as shown in Fig. 2C-a, -b, and -c, respectively. Since, in the case of EGFP, monomer protein exists and no specific interaction with other molecules could be detected in mammalian cells, one diffusion component is expected by FAF fitting. In order to confirm this theory, EGFP FAFs were also fitted by two- or three-component equations, respectively (Fig. 2C-b and -c). In the case of one-component fitting, the diffusion constant of EGFP was calculated as $2.6 \pm 0.4 \times 10^{-7}\,cm^2s^{-1}$ (Fig. 2C-a, Table 1). In the case of two- or three-component fittings, the distribution of the fraction which shows this diffusion constant is widely dispersed from 0% to 100% and diffusion constant values of fractions are from 10^{-9} to $10^{-5}\,cm^2s^{-1}$ (Fig. 2C-b and -c). The molecular weight of EGFP is 27 kDa and the expected diffusion constant is calculated as $2.5 \times 10^{-7}\,cm^2s^{-1}$ [11]. This diffusion constant is almost the same as the value calculated by one-component fitting. Therefore, EGFP is demonstrated to exist as a monomerical component in Hep3B cells. Since the value of its diffusion constant was almost the same in these fitting models, all the fitting models were useful for the analysis.

Analysis for localization of STAT3-GFP in living cells by FCS and statistical analysis of its diffusion constants

FAF for STAT3-GFP was measured with the same method as EGFP, as shown in Fig. 2. Positions for FCS measurement in Hep3B cells before and after IL-6 stimulation are shown in Figs. 3A and B, respectively. The value of $G(\tau)$ which shows the amplitude of the correlation curve by FAF significantly increased near the cytoplasmic membrane (Figs. 3C and D, closed triangle) in Hep3B cells after IL-6 stimulation. The value of $G(\tau)$ near the nucleic envelope and in nucleus slightly increased after IL-6 addition (Figs. 3C and D, closed and open circles). Before IL-6 addition, the value of $G(\tau)$ at the cytoplasmic membrane was higher than that at the other locations (Fig. 3C). Values of $G(\tau)$ especially near the cytoplasmic membrane and in the cytoplasm increased at 15 min after IL-6 stimulation. The reciprocal value of the y intercept (the value of $G(0)$) by FAF indicates the number of molecules in a detection area (see Eq. (1) in Materials and methods). These results suggested that the number of STAT3-GFP molecules at the cytoplasmic membrane and in cytoplasm was decreased by IL-6 stimulation. Two- and three-component models ($i = 2, 3$) were applied to these data (Figs. 3C–F) according to the criteria reported previously [12]. Briefly, first component model is associated with the diffusion constant of monomer STAT3, and second or third component model is associated with that of the complex form of STAT3 together with other proteins. The values of normalized it $G(\tau) - 1$ were calculated from those of $G(\tau)$ using the number of target proteins

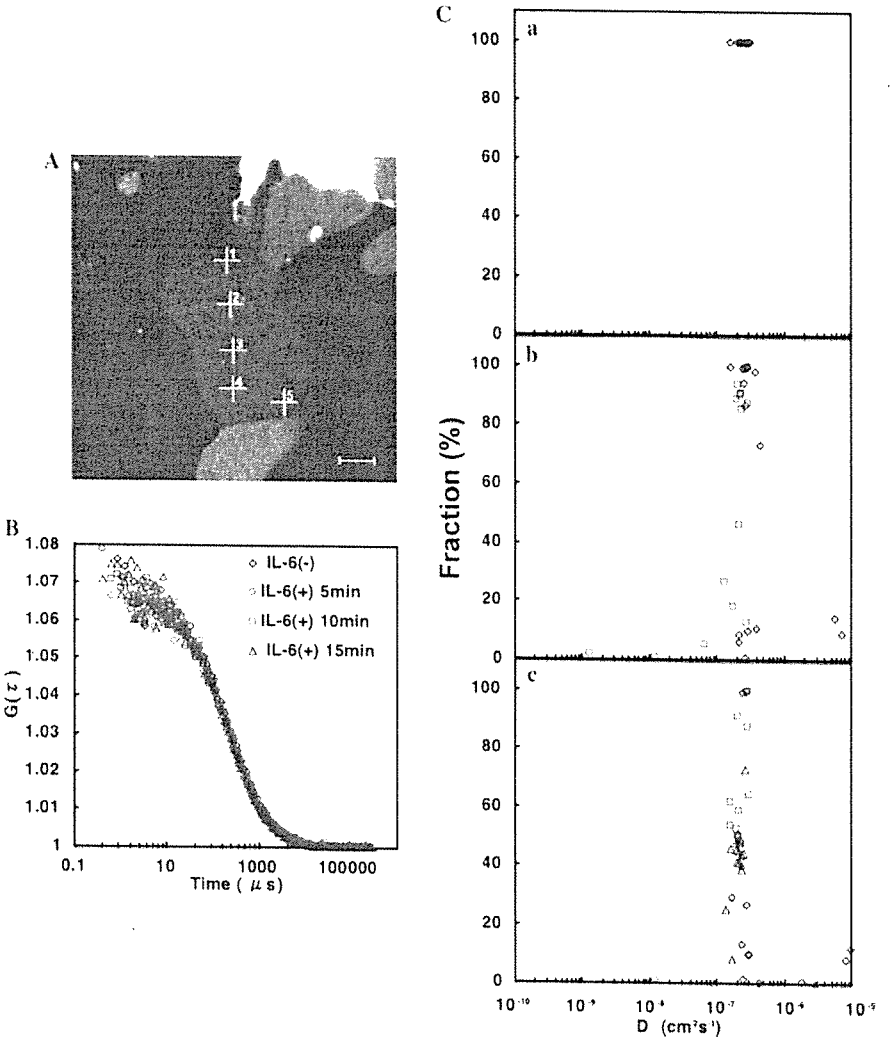

Fig. 2. Analysis of diffusion state of EGFP in Hep3B by IL-6 stimulation. (A) Hep3B cells were transfected with the expression vector of EGFP. Positions for FCS measurement are indicated by cross bars (1–5) in these transfected cells. Scale bar represents the length for 10 μm. (B) Analysis for FAF of EGFP after IL-6 stimulation at position 3 as shown in (A). (C) Scatter plots of diffusion constants (D) and fraction percentages (%). Each result of these data for one, two or three diffusion component fitting is shown in C-a, -b, and -c, respectively.

Table 1
Diffusion constant value and fraction ratio of EGFP in Hep3B cells after IL-6 stimulation

	n	$D(\tau)$ (cm^2s^{-1})	F (%)
IL-6 (−)	14	$2.6 \pm 0.4 \times 10^{-7}$	100
IL-6 (−) 5 min	12	$2.6 \pm 0.6 \times 10^{-7}$	100
IL-6 (−) 10 min	14	$2.5 \pm 0.6 \times 10^{-7}$	100
IL-6 (−) 15 min	15	$2.6 \pm 0.7 \times 10^{-7}$	100

Hep3B cells were transfected with the expression vector of EGFP. Diffusion constant value ($D(\tau)$) and fraction ratio (%) of EGFP in these transfected cells before and at 5, 10 or 15 min after IL-6 stimulation are shown. Number of the measured data in each case is shown in the line (indicated as n).

in the measured area, and are shown in Figs. 3E and F. Diffusion times of STAT3-GFP were almost the same at all measured positions of Hep3B cell before IL-6 addition (Fig. 3E). On the other hand, after IL-6 stimulation, the slowest diffusion components in the correlation curve appeared at the position in the nucleus (Fig. 3F, open circle). A slow diffusion component was also detected near the nucleic envelope and the cytoplasm (Fig. 3F, closed circle and open triangle).

Scatter plots of the diffusion constant and the fraction from FCS measurements of STAT3-GFP focusing on the cytoplasm and the area near the cytoplasmic membrane in Hep3B cells before and after IL-6 addition are shown in Fig. 4. Two- or three-component models were applied to these FAF data (Figs. 4C–F) according to the criteria reported previously [12].

The components with the highest percentage of the STAT3-GFP fraction were detected in the diffusion constant range of $1–5 \times 10^{-7}$ cm^2s^{-1}, near the cytoplasmic membrane, and also in the cytoplasm before IL-6 addi-

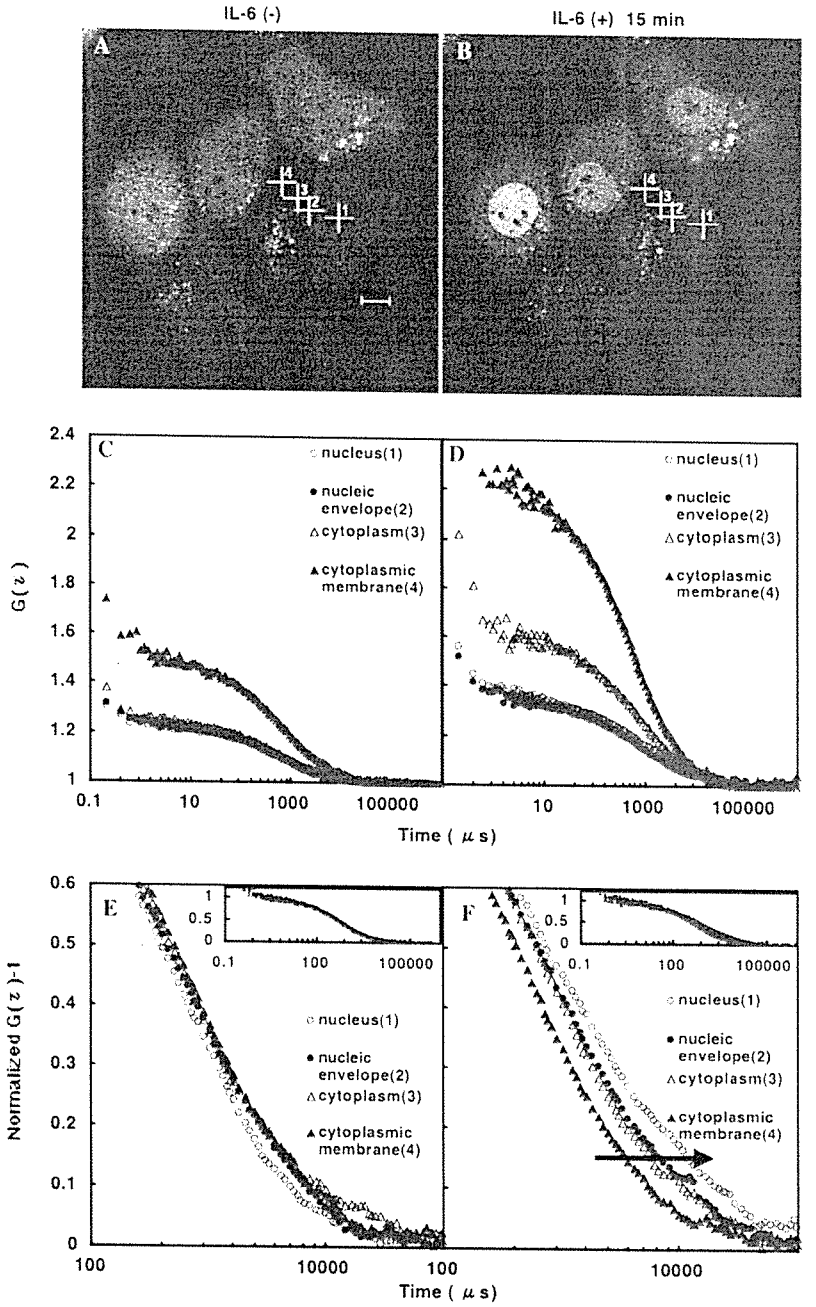

Fig. 3. Change of autocorrelation function of STAT3-GFP in Hep3B stable transformants. FCS measurements were carried out before (A, C, and E) and at 15 min after IL-6 stimulation (B, D, and F). Scale bar represents the length for 10 μm. Measured autocorrelation function before and after IL-6 stimulation is shown in C and D, respectively. Normalized autocorrelation function before and after IL-6 stimulation is shown in E and in F, respectively. Data for the full sized functions are shown in insets (in upper right panels).

tion (Figs. 4G and H). After IL-6 stimulation, the distribution of diffusion constants of STAT3 in the cytoplasmic membrane was dispersed in that of diffusion constant 1×10^{-8}–1×10^{-7} $cm^2 s^{-1}$ (Figs. 4D and G). These results suggested that IL-6 induced a change in the molecular complex state of STAT3 near the cytoplasmic membrane. The estimated diffusion constants of STAT3-GFP monomer from its molecular weight using the Einstein–Stokes equation was around 1.6×10^{-7} $cm^2 s^{-1}$, that of statosome I was 1.1–1.3×10^{-7} $cm^2 s^{-1}$ and that of statosome II was 6.1×10^{-8}–7.8×10^{-8} $cm^2 s^{-1}$. According to the above calculation, the main component of STAT3 in Hep3B cells before IL-6 stimulation is statosome I, the molecular weight of which is 200–400 kDa. It was also demonstrated that statosome II (1–2 MDa) complex was formed at the

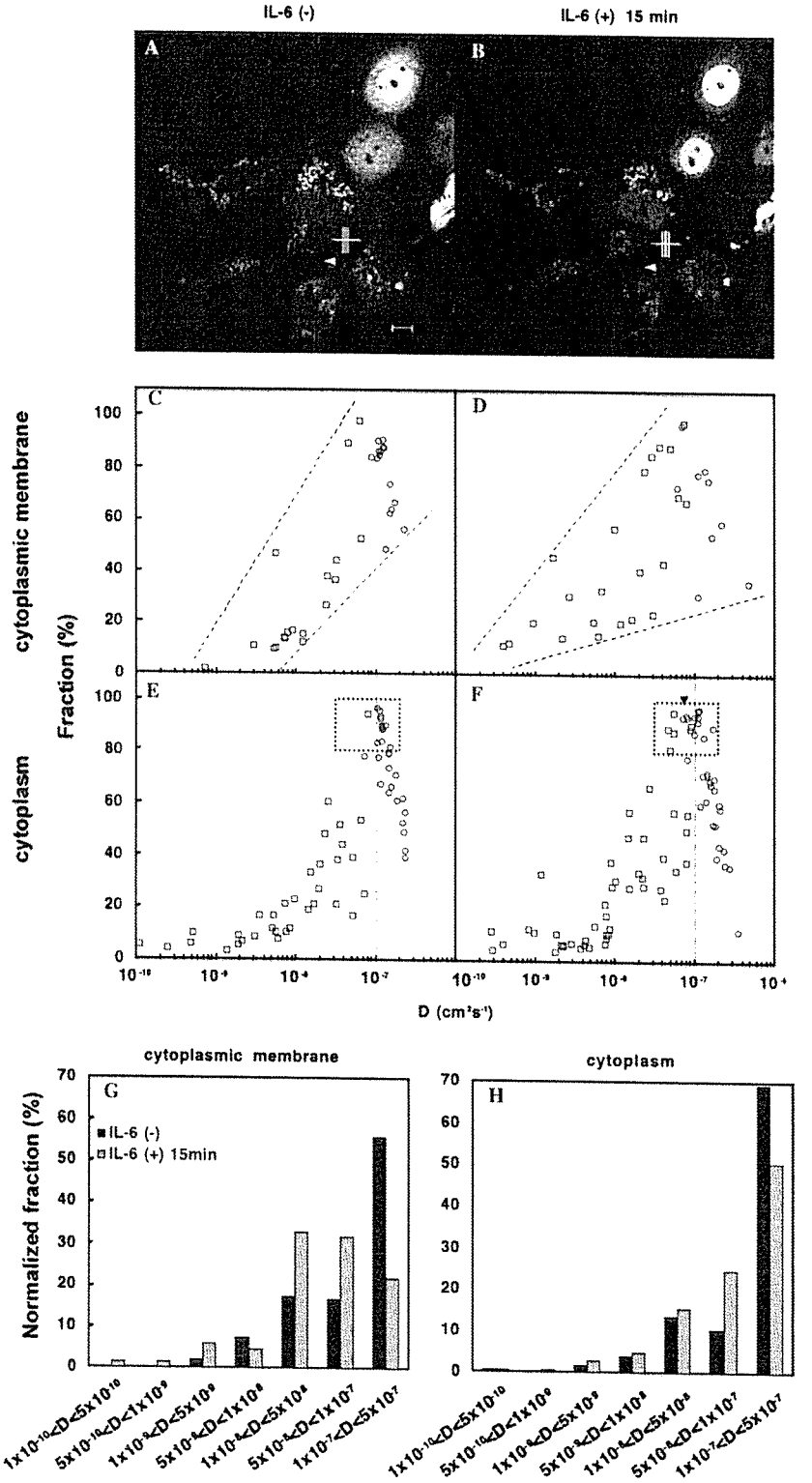

Fig. 4. Statistical analysis of diffusion constants at cytoplasmic membrane and in cytoplasm. Measurements of FAF were carried out at every 1 μm interval from cytoplasmic membrane to cytoplasm (A,B). Scatter dispersion plots of diffusion constants and their fractions from the data of FAF measurements for STAT3-GFP at cytoplasmic membrane (C,D) and in cytoplasm (E,F) before (C,E) and at 15 min after IL-6 stimulation (D,F). Difference of the area within the dotted lines in C or D shows a variance of diffusion constants at cytoplasmic membrane before and after IL-6 stimulation. Dashed line in E and F shows a ratio of the fraction at the value of diffusion constant of 1.0×10^{-7} cm^2s^{-1}. The area of the square dotted lines in E and F shows the fractions whose ratio was over 80%. Normalized fraction ratio (%) for each range (1.0×10^{-n}–5.0×10^{-n} and 5.0×10^{-n}–$1.0 \times 10^{-n+1}$ cm^2s^{-1}) of diffusion constant is shown in G and H.

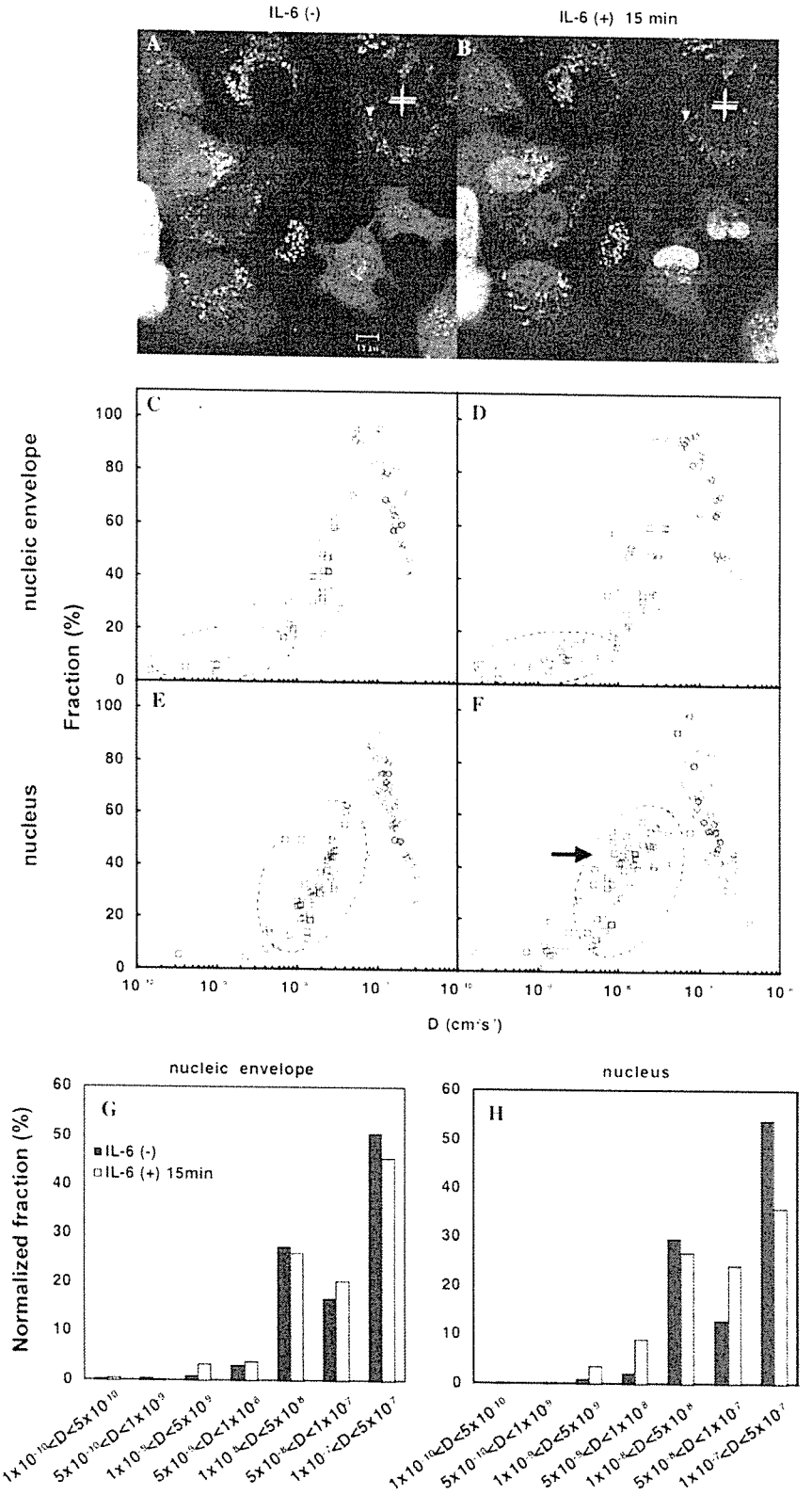

Fig. 5. Statistical analysis of diffusion constants at nucleic envelope and in nucleus. Measurements of FAF were carried out at every 1 μm interval from nucleic envelope into nucleus (A,B). Scatter plots of diffusion constants and their fractions from FAF measurements for STAT3-GFP at nucleic envelope (Figs. 4C and D) and in nucleus (Figs. 4E and F) before (Figs. 4C and E) and at 15 min after IL-6 addition (Figs. 4D and F). The area in the circle of dotted lines in (C)–(F) shows a fraction of main slow diffusion components. Normalized fraction ratio (%) for each range (1.0×10^{-n}–5.0×10^{-n} and 5.0×10^{-n}–$1.0 \times 10^{-n+1}$ cm^2s^{-1}) of diffusion constant is shown in G and H.

cytoplasmic membrane and in the cytoplasm after IL-6 stimulation.

On the other hand, most of the distribution of the diffusion constants at the nucleic envelope did not change before and after IL-6 stimulation (Figs. 5C, D, and G). However, an increase in components at very slow diffusion constants, less than $10^{-8}\,cm^2s^{-1}$, was observed after IL-6 stimulation (Fig. 5D, in the area enclosed by dashed line). This phenomenon presumably indicated that STAT3 that was present very close to the nucleic envelope might have been trapped by the outer nucleic envelope. In the nucleus, the ratio of the fraction of diffusion constants around 4.0×10^{-9}–$2.0\times10^{-8}\,cm^2s^{-1}$ increased (Fig. 5F, in dashed line area) and the ratio of diffusion components which show diffusion constants 1.0–$5.0\times10^{-7}\,cm^2s^{-1}$ decreased after IL-6 stimulation (Fig. 5H). These results demonstrated that the ratio of the distribution of STAT3 monomers decreased, and conversely, the ratio of STAT3 dimer complexes, which bind to the target DNA, was increased in the nucleus by IL-6 stimulation.

Discussion

Localization of STAT3-GFP and EGFP in Hep3B cells was measured by LSM before and after IL-6 addition. STAT3-GFP translocated from the cytoplasm to the nucleus, but no change of EGFP localization was observed in Hep3B cells after IL-6 addition (Fig. 1). These results were consistent with the previous data that STAT3 is translocated from the cytoplasm to the nucleus by IL-6 stimulation [27,28]. The results suggested that the GFP portion of STAT3-GFP did not affect the translocation of STAT3 by IL-6 stimulation. Furthermore, it was demonstrated that EGFP did not interact with intercellular structures and did not affect the molecular flow in Hep3B cells by the measurement of FAFs and analysis of diffusion constant (Fig. 2). Our data also showed that EGFP exists as a monomerical component in Hep3B cells.

FAF for STAT3-GFP was measured and the value of $G(\tau)$, which shows the amplitude of the correlation curve, increased near the cytoplasmic membrane in Hep3B cells after IL-6 stimulation (Figs. 3C and D). On the other hand, almost no change was observed in the amplitude of the correlation curves near the nucleic envelope and in the nucleus after IL-6 addition. IL-6 stimulation induced an increase in the values of $G(\tau)$ especially near the cytoplasmic membrane and in the cytoplasm. These results suggested that the number of STAT3 molecules present especially at the cytoplasmic membrane and in cytoplasm was decreased by IL-6 stimulation. These results were consistent with the data observed by LSM (Fig. 1). As shown in Fig. 3E, diffusion times of STAT3-GFP were almost the same at all measured positions of Hep3B cell before IL-6 addition. On the other hand, after IL-6 stimulation, the slowest diffusion components in the correlation curve appeared at the position in nucleus (Fig. 3F). Other slow diffusion components were also detected near the nucleic envelope, and cytoplasm. These results demonstrated that the diffusion speed of STAT3 present especially in the nucleus, at the nucleic envelope and in the cytoplasm was decreased by IL-6 stimulation. Recently, Stat3 has been shown to be enriched in dot-like structures within the nucleus [30], and this is consistent with our data.

Furthermore, statistical analysis of the diffusion constant of STAT3 (Figs. 4 and 5) was performed using the same criteria as in the case of EGFP. FCS measurement was carried out near the cytoplasmic membrane, in the cytoplasm, near the nucleic envelope, and in the nucleus before and after IL-6 stimulation. The presence of statosome I (in the size range of 200–400 kDa) and statosome II (1–2 MDa) was shown to exist in the cytosol as STAT3 complexes in Hep3B cells [24]. The expected diffusion constants according to the Einstein–Stokes equation of statosome I and statosome II were 1.1–$1.3\times10^{-7}\,cm^2s^{-1}$ and 6.1–$7.8\times10^{-8}\,cm^2s^{-1}$, respectively.

As shown in Figs. 4C and D, after IL-6 addition, the dispersion of STAT3-GFP diffusion constants and component fractions (%) near the cytoplasmic membrane was more spread out than that before IL-6 addition. It was demonstrated that the number of STAT3 complexes, whose molecular weight is around 200–400 kDa (diffusion constant, 1.0–$5.0\times10^{-7}\,cm^2s^{-1}$), decreased and that of STAT3 complex, whose molecular weight is more than 1 MDa (diffusion constant, 1.0×10^{-8}–$1.0\times10^{-7}\,cm^2s^{-1}$), increased at the cytoplasmic membrane after IL-6 stimulation (Fig. 4G). This result suggested that IL-6 stimulation induced the formation of STAT3 complex whose molecular size was larger than 1 MDa from STAT3 complex, whose molecular size was 400 kDa at the cytoplasmic membrane. When FCS was measured near the cytoplasmic membrane, photobleaching was often detected. This phenomenon indicates that recruitment and dissociation of STAT3 with gp130 and dimerization of STAT3 were induced near the cytoplasmic membrane.

The fraction of STAT3 complex of slow diffusion constants (5.0×10^{-8}–$1.0\times10^{-7}\,cm^2s^{-1}$) increased in the cytoplasm and the fraction of STAT3 complex, whose molecular weight was around 200–400 kDa (diffusion constant, 1.0×10^{-7}–$5.0\times10^{-7}\,cm^2s^{-1}$), decreased (Figs. 4F and H). These results demonstrated that the ratio of statosome I decreased and that of statosome II increased in the cytoplasm after IL-6 stimulation. It is suggested that these smaller complexes translocated into the nucleus and the ratio of the mega-complex of STAT3 increased in the cytoplasm. At the nucleic envelope, no change in the distribution of STAT3 complexes was apparent after IL-6 stimulation

(Fig. 5G). In the nucleus, the distribution of the fraction of slow diffusion components (diffusion constant, 5.0×10^{-8}–1.0×10^{-7} $cm^2 s^{-1}$) increased and the fraction of STAT3 complex, whose molecular weight is around 200–400 kDa (diffusion constant, 1.0–5.0×10^{-7} $cm^2 s^{-1}$), decreased (Fig. 5H). Interestingly, the distribution of very slow diffusion STAT3 complex (diffusion constant, 1.0×10^{-9}–1.0×10^{-8} $cm^2 s^{-1}$) increased only in the nucleus. This result demonstrated that IL-6 stimulation induced the formation of STAT3 complex that binds to the target DNA in the nucleus. The above results suggested that STAT3 dimerized, interacted with other proteins, and translocated from the cytoplasmic membrane to the nucleus after IL-6 stimulation.

In previous reports using conventional experimental methods, the state change of STAT3 complex forming large oligomer components by IL-6 stimulation in continuous time in a single living cell has not been shown [26–29].

In contrast, the results of our study demonstrate that STAT3 could form small and large megacomplexes before and after IL-6 stimulation, respectively, in Hep3B cells. Since GRP58, HSP90, and cav1 are reported to be associated with STAT3 in cytosol and plasma membrane raft [25,28], STAT3 might interact with other intracellular molecules through these molecules to form large complexes. Our results suggest that IL-6 stimulation induces the change in interaction of these molecules with STAT3 in the cytosol and plasma membrane raft. Furthermore, they suggest that the binding of STAT3 complex with the target DNA to form the complex showing very slow diffusion speed is induced by IL-6 stimulation only in nucleus.

In this study, we show that FCS is a powerful tool for biological experiments, because it has a spatio-temporal resolution that can be applied to the analysis of diffusion constant of molecules in living cells. We could carry out the measurement by LSM and FCS for IL-6 stimulated cells after 15 min. Measurements for these analyses with more shorter time course should be applied to analyze the mechanism for such receptor signaling and transcriptional activity via STAT3. However, since it needs several minutes for the measurement on one point in the cells by LSM and FCS, it needs more than 10 min for that on several measurement points. Measurement with more shorter time will be achieved using more faster or multi-point measurement system of FCS in the near future.

Moreover, it will be necessary to analyze with fluorescence cross correlation spectroscopy (FCCS) to actually verify how the statosome composition proteins interact with and dissociate from STAT3. FCCS is a measurement technique similar to FCS, but could be useful to assess the interaction state of two different fluorescence probes in a confocal observation field. To analyze with this technique, STAT3 and the target protein have to be fused to two different fluorescence proteins, for example, GFP and red fluorescence protein (RFP). Further research would advance the possibility of clarifying more precisely the binding state of STAT3 with other proteins in living cells by using FCS, FCSS, and other biological methods.

Acknowledgment

This work was supported by the Grant, 21st Century COE Program in Japan.

References

[1] R. Rigler, Ü. Mets, J. Widengren, P. Kash, Fluorescence correlation spectroscopy with high count rate and low background: analysis of translational diffusion, Eur. Biophys. J. 22 (1993) 169–175.

[2] M. Kinjo, G. Nishimura, T. Koyama, Ü. Mets, Single-molecule analysis of restriction DNA fragments using fluorescence correlation spectroscopy, Anal. Biochem. 260 (1998) 166–172.

[3] C.-G. Pack, G. Nishimura, M. Tamura, K. Aoki, H. Taguchi, M. Yoshida, M. Kinjo, Analysis of interaction between chaperonin GroEL and its substrate using fluorescence correlation spectroscopy, Cytometry 36 (1999) 247–253.

[4] Y. Takakuwa, C.-G. Pack, X.-L. An, S. Manno, E. Ito, M. Kinjo, Fluorescence correlation spectroscopy analysis of the hydrophobic interactions of protein 4.1 with phosphatidyl serine liposomes, Biophys. Chem. 82 (1999) 149–155.

[5] R. Brock, G. Vàmosi, G. Vereb, T.M. Jovin, Rapid characterization of green fluorescent protein fusion proteins on the molecular and cellular level by fluorescence correlation microscopy, Proc. Natl. Acad. Sci. USA 96 (1999) 10123–10128.

[6] P. Schwille, U. Haupts, S. Maiti, W.W. Webb, Molecular dynamics in living cells observed by fluorescence correlation spectroscopy with one- and two-photon excitation, Biophys. J. 77 (1999) 2251–2265.

[7] S. Terada, M. Kinjo, N. Hirokawa, Oligomeric tubulin in large transporting complex is transported via kinesin in squid giant axons, Cell 103 (2000) 141–155.

[8] R.H. Köhler, P. Schwille, W.W. Webb, M.R. Hanson, Active protein transport through plastid tubules: velocity quantified by fluorescence correlation spectroscopy, J. Cell Sci. 113 (2000) 3921–3930.

[9] N. Yoshida, M. Kinjo, M. Tamura, Microenvironment of endosomal aqueous phase investigated by the mobility of microparticles using fluorescence correlation spectroscopy, Biochem. Biophys. Res. Commun. 280 (2001) 312–318.

[10] Y. Nomura, H. Tanaka, L. Peollinger, F. Higashino, M. Kinjo, Monitoring of in vitro and in vivo translation of green fluorescent protein and its fusion proteins by fluorescence correlation spectroscopy, Cytometry 44 (2001) 1–6.

[11] K. Saito, E. Ito, Y. Takakuwa, M. Tamura, M. Kinjo, In situ observation of mobility and anchoring of PKCL1 in plasma membrane, FEBS Lett. 541 (2003) 126–131.

[12] T. Kishimoto, Signal transduction through homo- or heterodimers of gp130, Stem Cell 12 (1994) 37–45.

[13] D. Guschin, N. Rogers, J. Briscoe, B. Witthuhn, D. Watling, F. Horn, S. Pellegrini, K. Yasukawa, P. Heinrich, G.R. Stark, et al., A major role for the protein tyrosine kinase JAK1in the JAK/STAT signal transduction pathway in response to interleukin-6, EMBO J. 14 (7) (1995) 1421–1429.

[14] Y. Yamanaka, K. Nakajima, T. Fukuda, M. Hibi, T. Hirano, Differentiation and growth arrest signals are generated through the cytoplasmic region of gp130 that is essential for Stat3 activation, EMBO J. 15 (7) (1996) 1557–1565.

[15] M. Minami, M. Inoue, W. Shi, K. Takeda, M. Matsumoto, T. Kishimoto, S. Akira, STAT3 activation is a critical step in gp130-mediated terminal differentiation and growth arrest of a myeloid cell line, Proc. Natl. Acad. Sci. USA 93 (1996) 3963–3966.

[16] C. Gerhartz, B. Heesel, J. Sasse, U. Hemmann, C. Landgraf, J. Schneider-Mergener, F. Horn, P.C. Heinrich, L. Graeve, Differential activation of acute phase response factor/STAT3 and STAT1 via the cytoplasmic domain of the interleukin 6 signal transducer gp130, J. Biol. Chem. 22 (1996) 12991–12998.

[17] U. Hemman, C. Gerhartz, B. Heesel, J. Sasse, G. Kurapkat, J. Grötzinger, A. Wollmer, Z. Zhong, J.E. Darnell Jr., L. Graeve, P.C. Heinrich, F. Horn, Differential activation of acute phase response factor/Stat3 and Stat1 via the cytoplasmic domain of the interleukin 6 signal transducer gp130, J. Biol. Chem. 22 (1996) 12999–13007.

[18] L.D. Ward, A. Hammacher, G.J. Howlett, J.M. Matthews, L. Fabri, R.L. Moritz, E.C. Nice, J. Weinstock, R.J. Simpson, Influence of interleukin-6 (IL-6) dimerization on formation of the high affinity hexameric IL-6z receptor complex, J. Biol. Chem. 23 (1996) 20138–20144.

[19] M. Inoue, M. Minami, M. Matumoto, T. Kishimoto, S. Akira, The amino acid residues immediately carboxyl-terminal to the tyrosine phosphorylation site contribute to interleukin 6-specific activation of signal transducer and activator of transcription 3, J. Biol. Chem. 14 (1997) 9550–9555.

[20] P.C. Heinrich, I. Behrmann, G. Müller-Newen, F. Schaper, L. Graeve, Interleukin-6-type cytokine signalling through the gp130/Jak/STAT pathway, Biochem. J. 334 (1998) 297–314.

[21] J.E. Darnell Jr., STATs and gene regulation, Science 277 (1997) 1630–1635.

[22] A.K. Kretzschmar, M.C. Dinger, C. Henze, K. Brocke-Heidrich, F. Horn, Analysis of Stat3 (signal transducer and activator of transcription 3) dimerization by fluorescence resonance energy transfer in living cells, Biochem. J. 377 (Pt. 2) (2004) 289–297.

[23] A.L. Pranada, S. Metz, A. Herrmann, P.C. Heinrich, G. Muller-Newen, Real time analysis of STAT3 nucleocytoplasmic shuttling, J. Biol. Chem. 279 (15) (2004) 15114–15123.

[24] M.I. Ndubuisi, G.G. Guo, V.A. Fried, J.D. Etlinger, P.B. Sehgal, Cellular physiology of STAT3: where's the cytoplasmic monomer?, J. Biol. Chem. 36 (1999) 25499–25509.

[25] T. Okamoto, A. Schlegel, P.E. Scherer, M.P. Lisanti, Caveolins, a family of scaffolding proteins for organizing "preassembled signaling complexes" at the plasma membrane*, J. Biol. Chem. 10 (1998) 5419–5422.

[26] G.G. Guo, K. Patel, V. Kumar, M. Shah, V.A. Fried, J.D. Etlinger, P.V. Sehgal, Association of the chaperone glucose-regulated protein 58 (GRP58/ER-60/ERp57) with Stat3 in cytosol and plasma membrane complexes, J. Interferon Cytokine Res. 22 (2002) 555–563.

[27] P.B. Sehgal, G.G. Guo, M. Shah, V. Kumar, K. Patel, Cytokine signaling stats in plasma membrane rafts, J. Biol. Chem. 14 (2002) 12067–12074.

[28] M. Shah, K. Patel, V.A. Fried, P.B. Sehgal, Interactions of STAT3 with caveolin-1 and heat shock protein 90 in plasma membrane raft and cytosolic complexes, J. Biol. Chem. 47 (2002) 45662–45669.

[29] N. Sato, T. Yamamoto, Y. Sekine, T. Yumioka, A. Junicho, H. Fuse, T. Matsuda, Involvement of heat-shock protein 90 in the interleukin-6-mediated signaling pathway through STAT3, Biochem. Biophys. Res. Commun. 300 (2003) 847–852.

[30] A. Herrmann, U. Sommer, A.L. Pranada, B. Giese, A. Kuster, S. Haan, W. Becker, P.C. Heinrich, G. Muller-Newen, STAT3 is enriched in nuclear bodies, J. Cell Sci. 117 (Pt. 2) (2004) 339–349.

THE JOURNAL OF BIOLOGICAL CHEMISTRY

Vol. 279, No. 20, Issue of May 14, pp. 21533–21542, 2004
Printed in U.S.A.

Regulation of Immature Protein Dynamics in the Endoplasmic Reticulum*

Received for publication, February 9, 2004, and in revised form, February 19, 2004
Published, JBC Papers in Press, February 19, 2004, DOI 10.1074/jbc.M401403200

Asako Kamada‡§, Hisao Nagaya§¶, Taku Tamura§¶, Masataka Kinjo‖, Hai-Ying Jin‡, Toshiharu Yamashita‡, Kowichi Jimbow‡, Hideo Kanoh, and Ikuo Wada§¶‡‡**

*From the Departments of ‡Dermatology and **Biochemistry, Sapporo Medical University School of Medicine, Sapporo 060-8556, Japan, the §Core Research for Evolutional Science and Technology, JST, Japan, the ¶Department of Cell Science, Institute of Biomedical Sciences, Fukushima Medical University School of Medicine, Fukushima 960-1295 Japan, and the ‖Research Institute for Electronic Science, Hokkaido University, Sapporo 060-0812, Japan*

The quality of nascent protein folding *in vivo* is influenced by the microdynamics of the proteins. Excessive collisions between proteins may lead to terminal misfolding, and the frequency of protein interactions with molecular chaperones determines their folding rates. However, it is unclear how immature protein dynamics are regulated. In this study, we analyzed the diffusion of immature tyrosinase in the endoplasmic reticulum (ER) of non-pigmented cells by taking advantage of the thermal sensitivity of the tyrosinase. The diffusion of tyrosinase tagged with yellow fluorescence protein (YFP) in living cells was directly measured using fluorescent correlation spectroscopy. The diffusion of folded tyrosinase in the ER of cells treated with brefeldin A, as measured by fluorescent correlation spectroscopy, was critically affected by the expression level of tyrosinase-YFP. Under defined conditions in which random diffusional motion of folded protein was allowed, we found that the millisecond-order diffusion rate observed for folded tyrosinase almost disappeared for the misfolded molecules synthesized at a nonpermissive high temperature. This was not because of enhanced aggregation at the high temperature, as terminally misfolded tyrosinase synthesized in the absence of calnexin interactions showed comparable, albeit slightly slower, diffusion. Yet, the thermally misfolded tyrosinase was not immobilized when measured by fluorescence recovery after photobleaching. In contrast, terminally misfolded tyrosinase synthesized in cells in which α-glucosidases were inhibited showed extensive immobilization. Hence, we suggest that the ER represses random fluctuations of immature tyrosinase molecules while preventing their immobilization.

The maturation of proteins in the secretory pathway requires various sequential reactions including suppression of backward movements through the translocational channel by BiP (1); cleavage of the signal sequence and attachment of *N*-linked oligosaccharides (2); the prevention of nonproductive folding intermediates by various molecular chaperones (3); disulfide shuffling by disulfide isomerases possessing chaperone activity (4, 5); and proline isomerization (6). When these processes are not completed, proteins are disposed eventually. Recent extensive studies have been revealing the underlying molecular mechanisms of this destruction (7–11). However, there are also misfolded proteins that are able to maintain reversible folding for several hours after synthesis but somehow fail to exit the ER.[1] A temperature-sensitive ts045 variant of the vesicular stomatitis virus glycoprotein (VSVG) is the best known example (12–14). It was thought that the defect in the exit of this glycoprotein from the ER and its transport to the Golgi could be explained by (*a*) uncompleted interactions of cargo proteins with the "ER matrix," which is composed of various chaperones and folding enzymes (15, 16) or (*b*) misfolded aggregates (13) that are too large to enter the COPII-coated ER exit sites. However, measurements of the misfolded VSVG mutant in living cells using fluorescence recovery after photobleaching (FRAP) (17) surprisingly showed that the thermal-induced misfolding caused no significant loss of lateral mobility (18). While various models can be conceived to explain the results, the study at least eliminated the possibility that the misfolded VSVG failed to exit because it is tethered to the immobile ER matrix (19).

Movements of newly synthesized proteins could affect their folding *per se*. Collision of two molecules exposing hydrophobic patches on their surfaces could result in the formation of aggregates. Also, folding rates depend on the frequency of collision with molecular chaperones. Hence, it is expected that the mobility of proteins during folding is regulated in living cells. However, this is hard to measure by FRAP because FRAP records the average motion of a mass population and its time resolution is not sufficient for complicated dynamics including submillisecond diffusion. For measuring such random diffusional motion of an individual protein, fluorescence correlation spectroscopy (FCS) is, at present, the only practical method (20–22). FCS detects fluctuation of the fluorescence intensity in a confocally defined volume with a sharply focused laser. This method has been developed as a unique technique to measure translational and rotational diffusion coefficients of molecules in solution and in living cells (22–25). Application of this technique to biological systems has brought to light novel aspects of various molecular dynamisms, such as the status of the tubulin complex in kinesin-mediated axonal transport in the squid giant axon (26). However, this method has not been used to

* This work was supported by grants from the Ministry of Education, Science, Sports and Culture of Japan (to I. W.). The costs of publication of this article were defrayed in part by the payment of page charges. This article must therefore be hereby marked "*advertisement*" in accordance with 18 U.S.C. Section 1734 solely to indicate this fact.

‡‡ To whom correspondence should be addressed: Dept. of Cell Science, Institute of Biomedical Sciences, Fukushima Medical University School of Medicine, Fukushima 960-1295 Japan. Tel.: 81-24-547-1663; Fax: 81-24-549-8898; E-mail: iwada@fmu.ac.jp.

[1] The abbreviations used are: ER, endoplasmic reticulum; CFP, cyan fluorescent protein; FCS, fluorescence correlation spectroscopy; FRAP, fluorescence recovery after photobleaching; YFP, yellow fluorescent protein; DOPA, dihydroxyphenylalanine; VSVG, vesicular stomatitis virus glycoprotein.

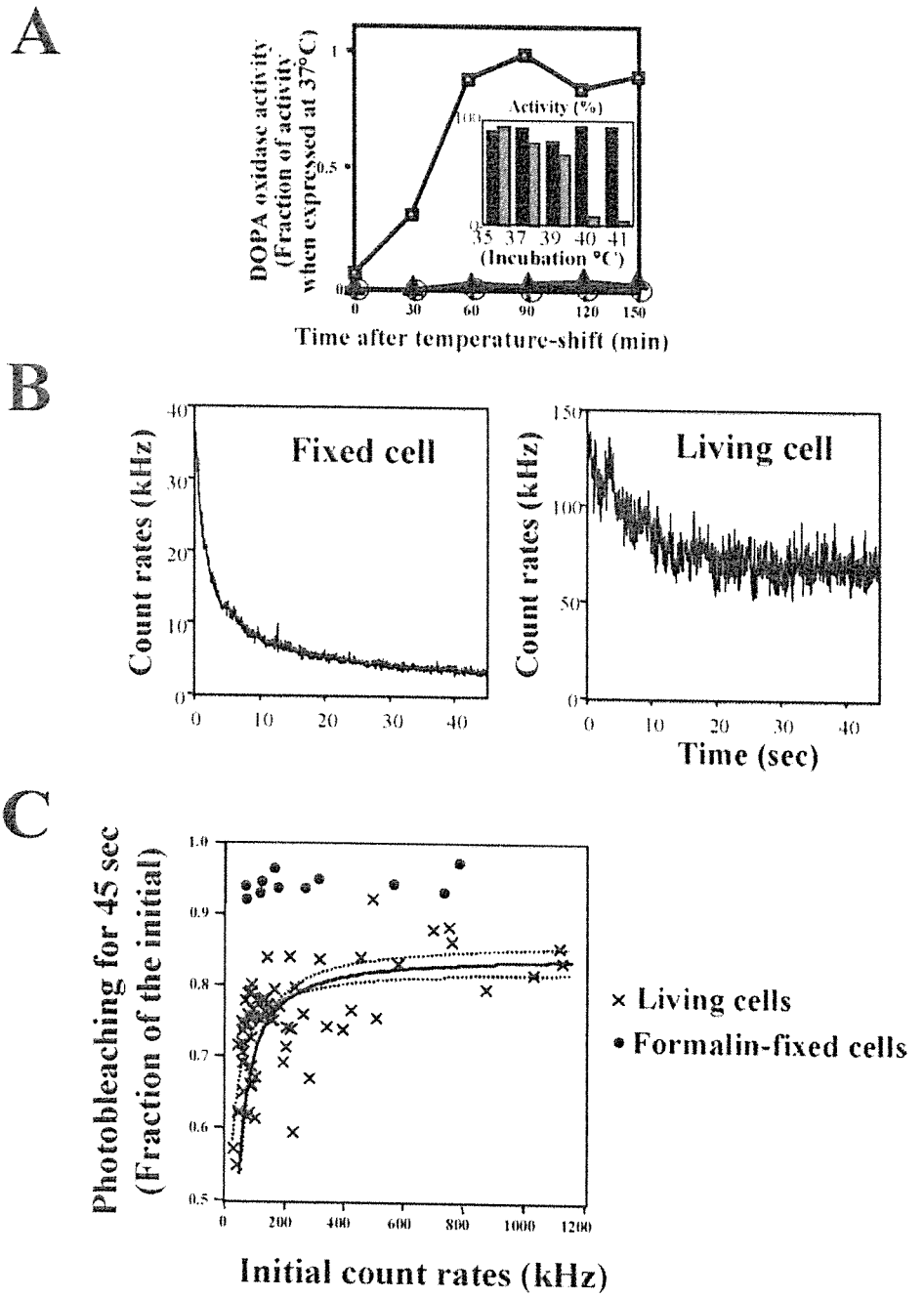

FIG. 1. **Determination of conditions for measuring the diffusional mobility of tyrosinase using FCS.** *A*, thermal synchronization of tyrosinase folding. SiHa cells infected with a recombinant adenovirus expressing wild type tyrosinase were incubated at 40 °C for 24 h and then incubated at 37 °C for the indicated periods in the presence of 40 μM puromycin. *Squares*, complete medium; *circles*, ATP-depleted medium; *triangles*, medium with an α-glucosidase inhibitor, castanospermine. *Inset*, *shaded bars*, sensitivity of folding to the culture temperature. Tyrosinase was expressed at the indicated temperatures for 24 h. *Black bars*, stability of mature tyrosinase. Tyrosinase was expressed at 37 °C for 24 h, then incubated at the indicated temperature with 40 μM puromycin for 24 h. The cells were lysed, then the DOPA oxidase activity of the lysates was measured. The amounts of tyrosinase in the lysates were determined by immunoblots. The enzyme activity was expressed as relative activity per immunoreactive tyrosinase. The average of three experiments is shown. *B*, fluorescence intensity (count rate) of tyrosinase-YFP before (*right*) and after (*left*) fixation. An expression vector for tyrosinase-YFP was used to coat beads that were then loaded into COS7 cells and incubated in the presence of brefeldin A (5 μg/ml) for 2 h at 37 °C. The fluorescent signal in a spot in the ER was then counted for 45 s in the living cells (*right*) or recorded in the same medium after fixation with 3.7% formalin for 10 min at 37 °C (*left*). *C*, photobleaching is affected by expression levels. Tyrosinase-YFP was expressed as in *B* and the fluorescence signal of spots in cells was measured. The degree of photobleaching for 45 s was calculated according to the equation: $(I_{ini} - I_{min})/I_{ini}$, where I_{ini} is the initial rate and I_{min} the minimum rate during a 45-s recording period (×, living cells; *dots*, fixed cells). Assuming that the relationship fits with the saturation binding curve, the best-fitting curve was determined using PRISM software. The area of 95% confidence is indicated by the *dotted lines*.

analyze the process of protein maturation in living cells.

To study the dynamics of immature proteins, we reasoned that we might be able to use the thermal sensitivity of tyrosinase, a melanosomal membrane enzyme catalyzing the oxidation of monohydric phenols, a critical step in melanin biosynthesis (EC 1.14.18.1) (27). Failure to express its catalytic

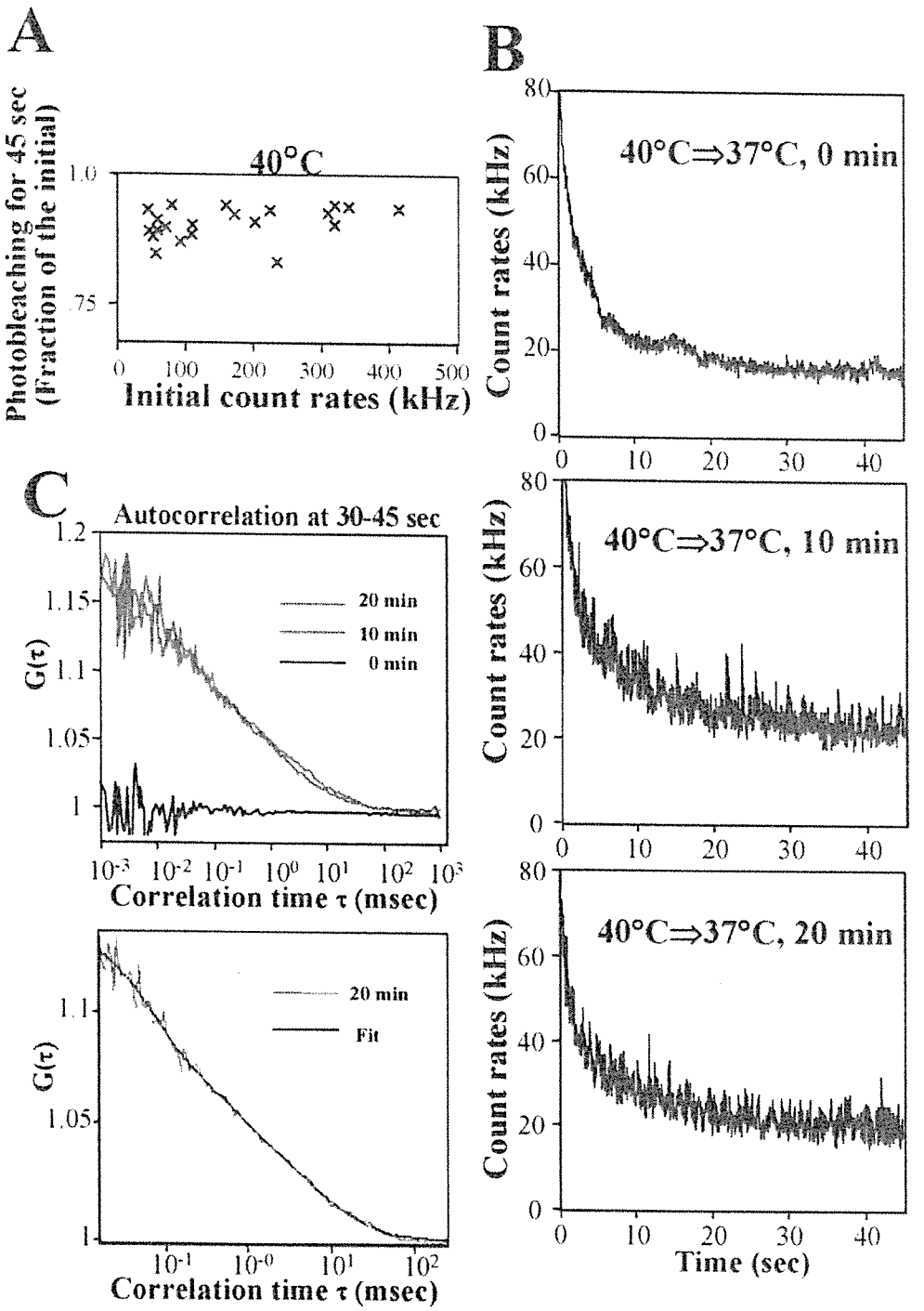

FIG. 2. **FCS measurements of thermally misfolded tyrosinase.** Tyrosinase-YFP was expressed at 40 °C for 2 h and its diffusional motion in the ER was measured by FCS. *A*, photobleaching of thermally misfolded tyrosinase. The photobleached fraction was plotted against the expression levels as in Fig. 1*C*. In this case, the photobleached fraction does not depend on the initial intensity. *B*, changes in fluorescence fluctuation upon temperature shift. Immediately after synthesis at 40 °C for 2 h, fluorescence was recorded in the ER for 45 s (*top*). The same cells were then incubated on the microscopic stage at 37 °C in the presence of 40 μM puromycin and the fluorescence of the same spot was recorded at 10 (*middle*) and 20 min (*bottom*). *C*, autocorrelation function of *B*. Autocorrelation function of the last 15 s of the recording period is shown at 0 (*top panel, black line*), 10 (*green line*), and 20 min (*black line*) after the temperature shift to 37 °C. Thermally misfolded tyrosinase showed little autocorrelation (*top panel, black line*). The best-fit two-component simulation profile (T = 0.64 ms, 50.7% and T = 9.16 ms, 49.3%) of the obtained autocorrelation function data at 20 min is shown in the *bottom panel* (*black line*).

activity results in the occurrence of oculocutaneous albinism type I (28). Pigment cells from individuals with some types of this disorder are temperature-sensitive (29, 30). When wild type tyrosinase is expressed in non-pigmented cells, its folding is also sensitive to heat (31). Completion of tyrosinase folding is a well defined step in that it can be monitored by the acquisition of dihydroxyphenylalanine (DOPA) oxidizing activity either *in situ* or in solution, and it depends entirely on interactions with calnexin (32–35). In non-pigmented cells, tyrosinase is transported to endosomal/lysosomal vesicles (36–40). In this

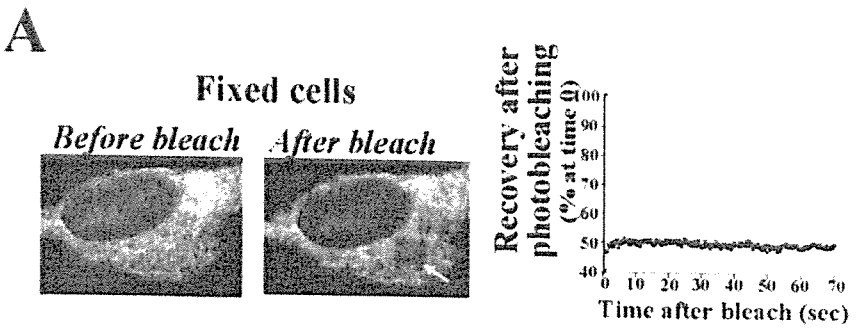

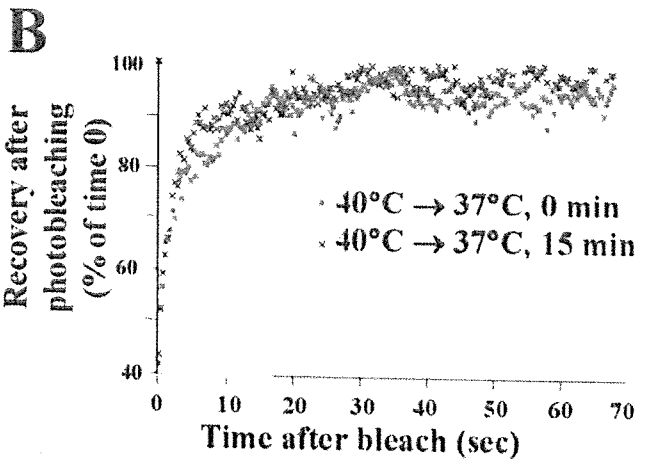

FIG. 3. **FRAP analysis.** Tyrosinase-YFP expression vector was bead loaded onto cells and expressed for 2 h at 40 °C. *A*, FRAP analysis was performed in a formalin-fixed cell. Images of the cell before and after FRAP are shown. The *arrow* indicates a photobleached region. *B*, FRAP analysis of a living cell. Recovery rates after photobleaching were measured in an adjacent area of the same single cell at 0 (*red*) or 15 min (*blue*) after a temperature shift to 37 °C in the presence of puromycin. *C*, summary of maximum recovery rates. FRAP was performed in only one region per cell to minimize loss of the mobile fraction by another round of FRAP. *n*, number of measurements.

C

Expression condition	Max recovery (%)
40°C → 37°C 0 min (n=20)	88.8 ± 7.9
40°C → 37°C 15 min (n=20)	90.4 ± 8.3

study we first tested whether the diffusion of folded tyrosinase is measurable. We then studied how the dynamics change in the thermally restricted condition. We also used FRAP to determine the fraction of the population that was immobilized. Our results show that folding appears to be regulated at various levels of microdynamics.

EXPERIMENTAL PROCEDURES

Expression Vectors and Culture Cells—The adenovirus vector used to express tyrosinase is described elsewhere (41). EcoRI and BamHI sites were attached to the human tyrosinase cDNA (35) by polymerase chain reaction (PCR). Tyrosinase fused to yellow fluorescent protein (YFP) or cyan fluorescent protein (CFP) was then produced by ligating the human tyrosinase into pEYFP-N1 or pECFP-N1 (BD Bioscience) cut with EcoRI and BamHI, respectively. For construction of the Sar1(T39N) expression vector, Sar1 cDNA was isolated by reverse transcription from HepG2 RNA using the primer 5′-GGATCAGTCCAGAGAAGTAAAAC-3′, then amplified by PCR with the pair of primers 5′-GCCGGAGAGCCCCTCAGGCCGTAGTAAGC-3′ and 5′-TCACCGTCCAAACATCAGTCAATATACTGG-3′. Restriction sites for BglII and KpnI were created at the 5′ and 3′ ends of the Sar1 cDNA using PCR. The Sar1 cDNA was then ligated into the corresponding sites of pEYFP-N1Δ whose EYFP open reading frame was removed by restriction with BamHI and NotI followed by ligation after polishing the terminus. To construct the GDP-restricted form of Sar1, the codon for Thr at amino acid 36 was mutated to that encoding Asn using the QuikChange™ protocol (Stratagene, La Jolla, CA). An expression vector for CFP-GT-(1–81) (GT-(1–81); the amino-terminal 81 amino acids of human β-1,4-galactosyltransferase) were purchased from Clontech. A vector for VSVG (ts045) was described previously (42). These vectors were introduced directly into cells using siliconized glass microbeads (42). SiHa and COS7 cells were obtained from the American Type Culture Collection (Manassas, VA). COS7 cells stably expressing hSec13-YFP were generated as follows. The coding sequence of human Sec13-YFP (42) was subcloned into the appropriate cloning sites of the retrovirus expression vector, pCX4bsr. pCX4bsr, a generous gift from Dr. T. Akagi (Osaka BioScience Institute), is a modified version of pCXbsr (43) that lacks the internal initiation codons within the gag region. The recombinant retrovirus was generated as described (43) and used to infect COS7 cells. The cells expressing hSec13 were selected by culturing them in Dulbecco's modified Eagle's medium containing blasticidin (10 μg/ml).

Analysis of Protein Dynamics in Living Cells—Live cell analysis using the microscopy was essentially described previously (42). The culture temperature of cells on the microscope stage was controlled using an objective heater for a planapochromat lens ×63 (Bioptechs, Butler, PA) or a Silicon Heater (Cell MicroControls, Norfolk, VA) for a C-Apochromat ×40 lens in combination with a stage heater (Kitazato Supply, Fujinomiya, Japan). To monitor the temperature of the cells

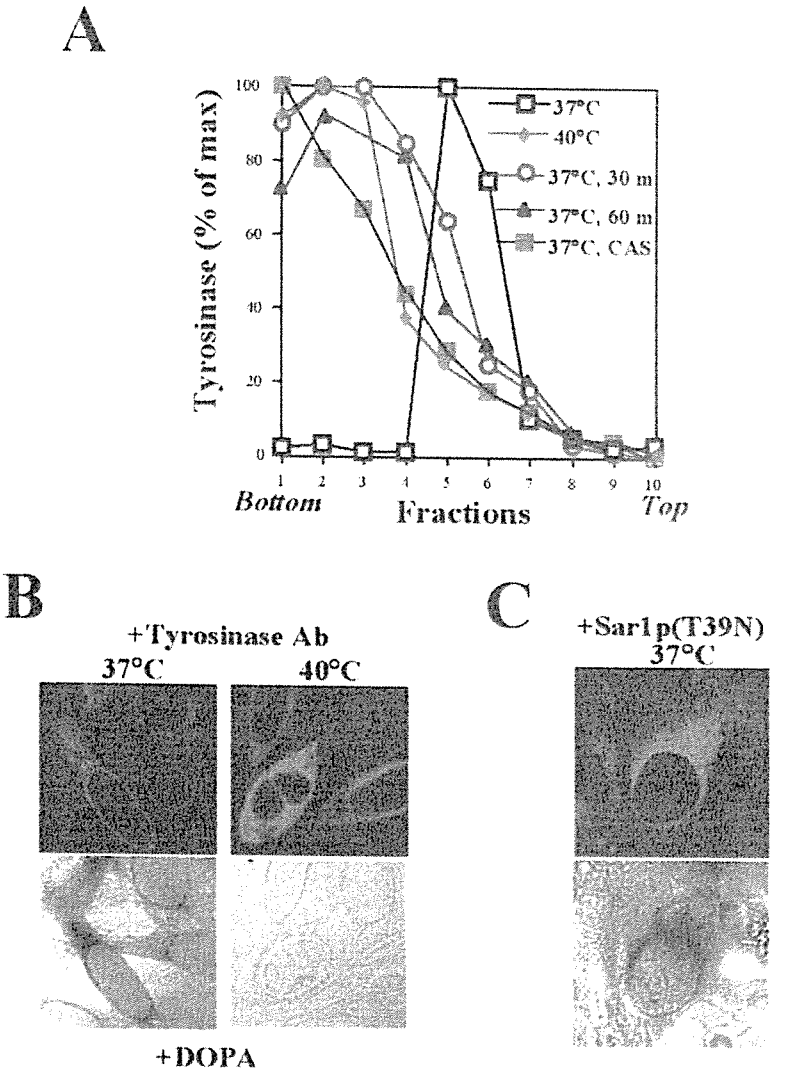

FIG. 4. **Characterization of tyrosinase maturation.** *A*, sedimentation velocity analysis of tyrosinase. Tyrosinase was expressed in SiHa cells at 37 (*black box*) or 40 °C (*other symbols*) for 24 h in the presence (*gray box*) or absence (*other symbols*) of 1 mM castanospermine, and then incubated at 37 °C with puromycin. Cells were lysed and applied to a sucrose gradient of 10–25%. The gradients were centrifuged and the fractions were collected from the bottom of the tube. As molecular mass markers, bovine serum albumin (5 S), catalase (11 S), and apoferritin (17 S) were recovered in fractions 8, 5–7, and 4–5, respectively. See "Experimental Procedures" for details. *B*, active staining of tyrosinase *in situ* at the non-permissive or the permissive temperature. Tyrosinase was expressed in SiHa cells at 37 (*left panels*) or 40 °C (*right panels*) for 24 h using recombinant adenovirus, and stained with anti-tyrosinase antibody (*top panels*) followed by an Alexa 488-labeled anti-mouse antibody or DOPA staining *in situ* (*bottom panels*) as described (35). Fluorescence (*top panels*) and transmission images (*bottom panels*) are shown. *C*, GDP-restricted form of Sar1 inhibits ER export of tyrosinase. The Sar1(T39N) expression vector was co-loaded into COS7 cells with the tyrosinase-YFP expression vector using glass beads. Tyrosinase-YFP fluorescence observed at 3 h post-loading was directly recorded and the active staining pattern was recorded as a transmission image.

under observation, an infrared thermometer (model CT820, CITIZEN Co., Tokyo, Japan) was used. For confocal microscopy and FCS analysis, a ConfoCor2 instrument (Zeiss, Jena, Germany) was used. Confocal images were taken with the laser scanning microscopy module. The excitation light of an argon ion laser at 514 nm was reflected by a dichroic mirror (HFT 514) and focused through a C-Apochromat ×40, NA = 1.2 water immersion objective (pinhole width 70 μm). A 530–560 nm band-pass filter was used to filter out the remaining scattered laser light. In all measurements, the minimum laser power of the setup was used. The fluorescence signal was recorded for three consecutive periods of 15 s (time resolution, 200 ns). The autocorrelation function and data fitting was performed with the software provided with the setup. Indirect immunofluorescence of fixed cells and time-lapse analysis of fluorescent molecules in live cells were carried out and processed as described previously by Nagaya *et al.* (42). For FRAP experiments, an area (1 μm^2) was exposed to the maximum power of the argon laser and then the recovery from the bleaching was measured at the minimum power of the laser. The obtained data were analyzed by fitting to a formula for one-dimensional diffusion (44) using Prism version 3.0 software (San Diego, CA).

Tyrosinase Activity Measurements and Sedimentation Analysis—Active staining of DOPA oxidase and spectrophotomeric measurements of DOPA oxidase activity in cellular lysates were carried out as described (35). To determine the sedimentation velocity of tyrosinase synthesized under various culture conditions, cells in a 60-mm dish were lysed with 0.5 ml of 1% sodium cholate, 0.15 M NaCl, 20 mM potassium phosphate, pH 7.2, and directly loaded onto a sucrose gradient from 25 to 10% in 0.3% sodium cholate, 0.15 M NaCl, 20 mM potassium phosphate, pH 7.2, in a tube for a Hitachi RPS40T rotor. After centrifugation at 36,000 rpm for 18 h at 4 °C, ten 1-ml fractions were collected from the bottom of the tube and 10 μl from each fraction was subjected to immunoblot analysis using an anti-tyrosinase monoclonal antibody (Novocastra Laboratories Ltd., Balliol Business Park West, UK).

RESULTS

FCS Measurements of Tyrosinase Expressed in Non-pigmented Cells—To test whether we could use the reported thermal sensitivity of tyrosinase folding to synchronize its maturation, we first examined the heat lability of its folding and stability. A recombinant adenovirus was used to express tyrosinase in human cervical carcinoma SiHa cells for 24 h at 37 °C and at various other temperatures (Fig. 1*A*). For the cells incubated at 37 °C, protein synthesis was halted by the addition of puromycin and the cells were further incubated for 24 h at the indicated temperatures. The cells were then lysed with detergents and the DOPA oxidase activity was determined (35). The DOPA oxidase activity was dramatically reduced when tyrosinase was synthesized above 39 °C (Fig. 1*A*, *inset*). In contrast, thermal treatment of folded tyrosinase (*i.e.* tyrosinase synthesized at 37 °C) had little effects on the activity, indicating that completion of tyrosinase folding is arrested above 39 °C. Importantly, when the inactive tyrosinase formed at 40 °C was further incubated at 37 °C in the presence of puromycin, the protein became almost fully active with 60 min (Fig. 1*A*, *squares*). This activation was not observed in ATP-depleted medium (*circles*) or in the presence of an α-glucosidase inhibitor (*triangles*).

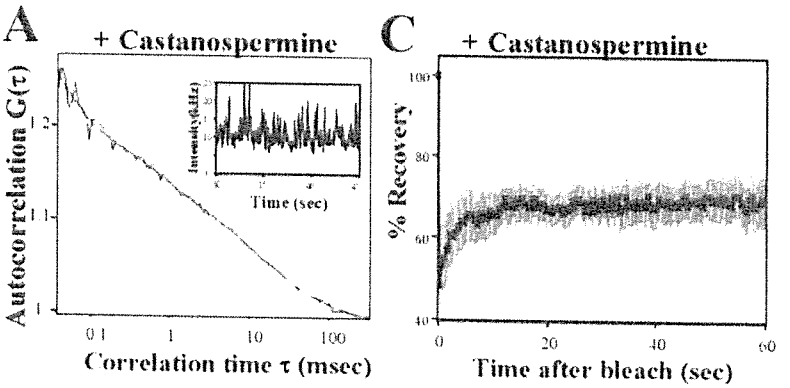

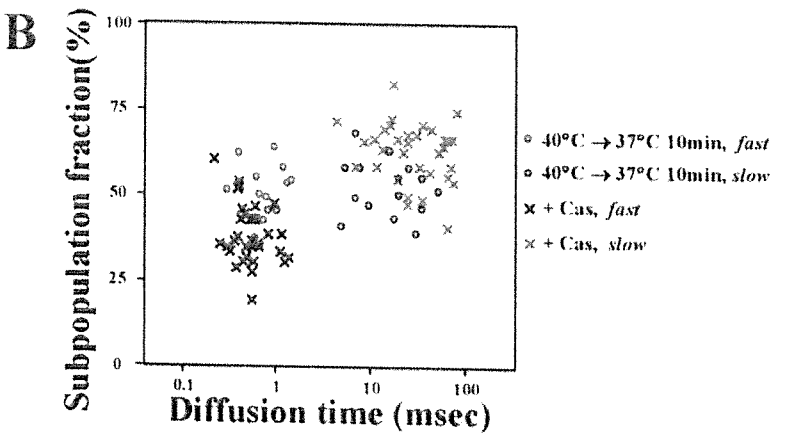

Expression condition	Diffusion time (msec) / (%) *Fast*	*Slow*
40°C (n=15)	N. D.	N. D.
40°C → 37°C 10 min (n=15)	0.768 ± 0.315 / (49.7 ± 7.6)	26.9 ± 16.7 / (41.7 ± 8.4)
+ CAS (n=33)	0.575 ± 0.275 / (37.8 ± 8.5)	46.1 ± 29.2 / (62.3 ± 8.6)

FIG. 5. **FCS and FRAP analysis of tyrosinase-YFP in castanospermine-treated cells.** Misfolded tyrosinase-YFP expressed in the presence of castanospermine at 37 °C for 2 h was subjected to FCS (*A*) or FRAP (*C*) analysis as described in the legends to Figs. 2 and 3, respectively. *Panel A*, best fitting two-component simulation profile (T = 0.59 ms, 45.6%, and T = 18.7 ms, 54.4%) (*black line*) and the autocorrelation function data (*blue line*). *Inset*, fluorescence fluctuation (the last 15 s of the recording period of three consecutive recordings) used for the autocorrelation analysis. *Panel B*, summary of FCS measurements. In the *upper panels*, fast and slow diffusion time in cells treated as indicated are plotted against the percentage of subpopulation estimated as in *panel A*. Averaged values and S.E. at each condition were calculated and are shown in the table. *N.D.*, not determined because of lack of autocorrelation. *Panel C*, recovery rates after photobleaching. The *error bars* are the measured S.E. (n = 6).

We then used this protocol to study how the mobility of tyrosinase is regulated during maturation. We reasoned that the diffusion profile of thermally misfolded tyrosinase may be distinct from the properly folded molecule if there is any regulation of mobility. To analyze mobility, we used FCS because this technique has the highest time resolution of the available techniques. However, it is known that FCS is often too sensitive to analyze cellular processes (21). In particular, photobleaching is a major obstacle. We therefore examined the conditions in which FCS could detect random diffusion in living cells. Because the degree of photobleaching obtained by FCS should correlate with the density of the molecules, we investigated which expression level would largely allow for random diffusion. In cells where the expression level is too high, the molecules would be at least partially immobilized. To achieve various levels of expression, we used siliconized glass microbeads (42). When photon-counting of tyrosinase-YFP was carried out in formalin-fixed cells, all fluorophores showed rapid decay of fluorescence to near background within 45 s, as expected (Fig. 1*B*, *left panel*). The fluctuation of the signal was almost at the level of noise, and no autocorrelation was observed from this counting (not shown). We next examined whether this setup could detect diffusion of tyrosinase-YFP expressed in a living cell at 37 °C for 2 h in the presence of brefeldin A, which prevents export from the ER (45). In this measurement, the degree of photobleaching was reduced compared with that in the fixed cells, and massive signal fluctuation was observed (Fig. 1*B*, *right panel*).

When we plotted the extent of bleaching, B, against the expression level, I_{ini}, we noticed that the relationship largely fits a simple saturable binding model: $B = B_{max} \cdot I_{ini}/(K + I_{ini})$. The constant K reflects the degree of correlation between photobleaching and the expression level. In the case of fixed cells, K should be ~0. If the level of tyrosinase expression has little influence on diffusional motion in the membrane, K should far exceed I_{ini}. This would happen if the fluorophore is very bright, so that the number of expressed molecules is very small. However, when measured in the living cells, this is not the case. In the living cells, a significant correlation was observed between the two values when the initial count rate was below 100 kHz (Fig. 1*C*, ×), suggesting that at least tyrosinase-YFP was not saturated at this range and, thus, random diffusion of tyrosinase-YFP should be measurable.

Regulation of Diffusional Mobility of Thermally Misfolded Tyrosinase—We next expressed tyrosinase-YFP at 40 °C and plotted the degree of photobleaching against the number of misfolded molecules. Surprisingly, massive photobleaching was observed irrespective of the expression level (Fig. 2*A*). A typical decay curve is shown in Fig. 2*B* (*top panel*), which resembles that of the fixed protein (Fig. 1*B*). It should be noted

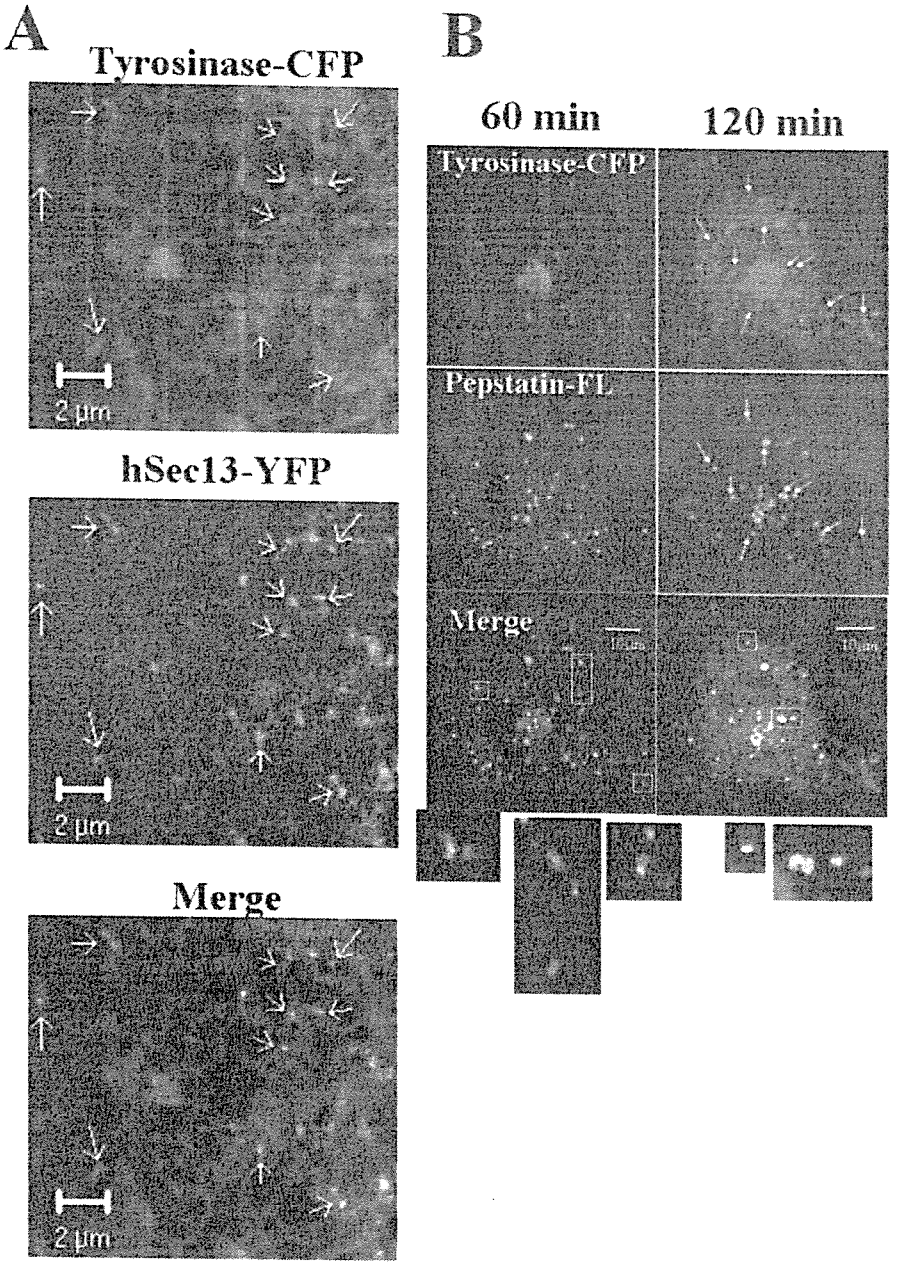

FIG. 6. **Targeting of tyrosinase-CFP in COS7 cells.** *A*, tyrosinase-CFP was concentrated in COPII-coated structures. Tyrosinase-CFP was expressed at 40 °C for 2 h in COS7 cells stably expressing hSec13-YFP. After the addition of puromycin, the cells were placed on a microscope stage and incubated at 37 °C. Shown are images in the ER network at 4 min. Most punctate structures containing tyrosinase-CFP (*red*) were coated with hSec13-YFP (*green*, *white arrows*). *B*, targeting of tyrosinase to lysosomes. Tyrosinase-CFP (*red*) was expressed as in *A* and incubated at 20 °C for 2 h in the presence of BODYPY-FL-labeled pepstatin (25 ng/ml, *green*) and puromycin. The medium was then changed to fresh medium without the labeled pepstatin and incubated for 1 or 2 h at 37 °C. At 1 h, most tyrosinase-containing structures were found in structures adjacent to pepstatin-positive vesicles, as shown in the enlarged images in the 60-min column. After incubation for another hour, most of the tyrosinase signals became completely merged with the fluorescent pepstatin signals, as shown in the enlarged images in the 120-min column.

that, different from the fixed cells, the decay in living cells reached a plateau at a significantly higher level than background (~1 kHz), suggesting the presence of a slow movement of nonbleached tyrosinase into the bleached area. However, this mobility was too slow to be captured by FCS. Nonetheless, the counting showed almost no autocorrelation over time (Fig. 2*C*, *black line*). To know if this lack of fluctuation is reversed when folding is allowed, we recorded the fluorescence in the same spot over a temperature shift from 40 °C (Fig. 2*B*, *top*) to 37 °C (Fig. 2*B*, *middle* and *bottom*). In these cases, fluctuation emerged upon temperature shift (Fig. 2*B*, *middle*). Interestingly, an almost identical autocorrelation curve was observed when incubation was continued at 37 °C for another 10 min (Fig. 2*C*, *red line*), except for a slight increase in the population with the faster mobility in the millisecond range. A two-component fitting analysis indicated that the mobility was composed of fast (T = 0.64 ms, 50.7%) and slow (T = 9.17 ms, 49.3%) diffusion components (Fig. 2*C*, *bottom panel*).

While these results indicated that the random diffusion detected by FCS was suppressed at 40 °C, they also suggested that the protein was slowly mobile at this temperature. We therefore examined whether such dynamics might be detected by FRAP. To test this possibility, we first assayed the rates of reversible photobleaching in fixed cells (46). An area of a formalin-fixed tyrosinase-YFP was photobleached by a pulse of intense laser beam, and the recovery rate was determined. As shown in Fig. 3*A*, the maximum laser beam reduced the signal to 42% of the initial level and within 1 s the intensity increased to 50% and remained there, suggesting that any recovery above 50% should be because of fluorophore exchange between the bleached and unbleached areas. We then determined the fraction of immobilized molecules in the living cells. While the fluorescence intensity of an area of tyrosinase-YFP synthesized for 2 h at 40 °C was reduced almost as much as it was in the fixed cell by an intense laser beam, the signal in the area recovered almost fully (Fig. 3*B*, *red*). Similarly, full recovery

from photobleaching was observed in the adjacent area when the cell was incubated on the stage at 37 °C for 15 min after 40 °C expression for 2 h although it appeared to be slightly faster (Fig. 3*B*, *blue*). These results and further independent experiments, as summarized in Fig. 3*C*, indicates that tyrosinase synthesized at 40 °C was slow, but fully mobile.

Diffusional Mobility of Aggregated Tyrosinase Formed in Castanospermine-treated Cells—To know whether the apparent lack of random diffusion seen with FCS measurements at non-permissive temperatures was because of the formation of large aggregates, we measured the molecular weight of detergent-solubilized tyrosinase using sedimentation analysis through sucrose density gradients. As shown in Fig. 4*A*, tyrosinase synthesized at the non-permissive temperature, 40 °C, was mostly found in the bottom three fractions of the gradient (*red line*). After 30 min at 37 °C, the majority was still found in the bottom fractions, but a slight increase in the recovery in fractions 4 and 5 was observed (*green line*). After 1 h at 37 °C, a small decrease in the percentage of tyrosinase in the bottom fraction was detected (*blue line*). An almost identical pattern was obtained at 2 h postincubation.[2] However, the molecules did not acquire the compact tertiary structure detected for the native enzyme synthesized without exposure to 40 °C (*black line*). When we examined terminally misfolded tyrosinase synthesized in the presence of an α-glucosidase inhibitor, castanospermine, the majority of the molecules were recovered in the bottom fractions, suggesting that they are largely aggregated. This analysis suggests that a slight alteration in size of tyrosinase aggregates is associated with the acquisition of activity, and that the thermally misfolded tyrosinase is structurally distinct from terminally misfolded tyrosinase.

To examine the possibility that the suppression of millisecond diffusion at the non-permissive temperature was caused by enhanced aggregation, we measured diffusion of the terminally misfolded tyrosinase synthesized in castanospermine-treated cells at 37 °C. However, in this case, the autocorrelation analysis showed that the diffusion of the slower mobility component was slightly slower but detectable by FCS (Fig. 5*A*). The typical measurement showed that the diffusion was composed of a fast (586.8 μs, 45.6%) and a slow (18.7 ms, 54.4%) diffusion (Fig. 5*A*). A summary of FCS measurements at various conditions is also shown in Fig. 5*B*. Hence, we conclude that the lack of autocorrelation at the non-permissive temperature was not the result of enlarged aggregates. However, FRAP analysis of the castanospermine-treated cells showed that the maximum recovery rate was reduced by ~30% (Fig. 5*C*). Taken together, we reasoned that long range diffusion, which is not observed in triglucosylated tyrosinase, is directly associated with the acquisition of the enzyme activity.

Enzymatically Active but Non-native Tyrosinase Was Transported to Lysosomes—Finally, we studied the fate of tyrosinase after a temperature shift to investigate whether the non-native but fully diffusible tyrosinase is properly targeted to lysosomes. The thermally misfolded tyrosinase was confined in the ER as expected (Fig. 4*B*). When a GDP-restricted form of Sar1, whose expression inhibits export of cargo from the COPII-coated ER exit sites, was co-expressed with tyrosinase at 37 °C, tyrosinase was retained in the ER and DOPA oxidase activity was expressed (Fig. 4*C*). Indeed, at 4 min after the temperature shift, at least some tyrosinase appeared to be concentrated in hSec13-coated structures (Fig. 6*A*). As shown in Fig. 7, time-lapse analysis revealed that transport to the Golgi apparatus, which was demarcated by coexpression of the Golgi marker

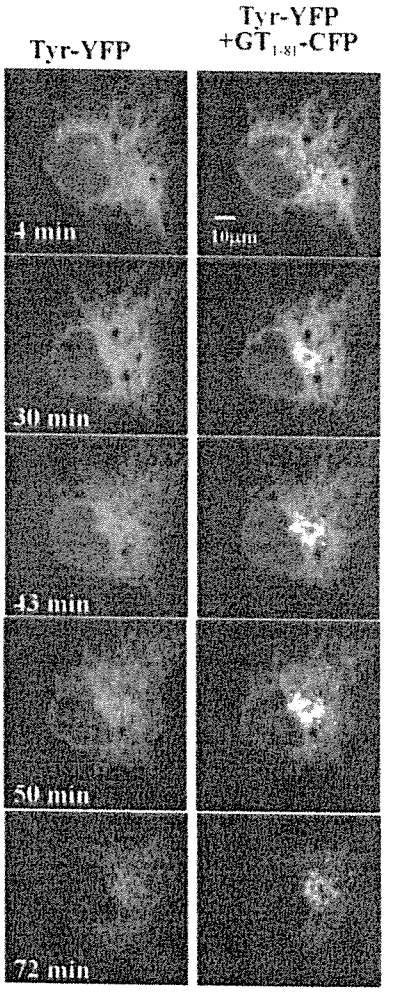

FIG. 7. **Transport of tyrosinase to lysosomes in a single cell.** Expression vectors for tyrosinase-YFP and CFP-GT-(1–81) were introduced into COS7 cells by siliconized glass microbeads and incubated for 2 h at 40 °C. The temperature was lowered to 37 °C after the addition of 40 μM puromycin and then both fluorescent images were recorded at 20-s intervals. The *green* images represent tyrosinase-YFP and the *red* images represent CFP-GT-(1–81) in the same cell.

galactosyltransferase-(1–81)-CFP, was clearly observed at 30 min after a temperature shift from 40 to 37 °C (Fig. 7, *red*). Further incubation allowed the initial formation of small vesicles at 50 min and of large granules at 72 min. The larger granules were identified as lysosomes because tyrosinase colocalized with lgp85 within them.[2] Interestingly, tyrosinase was found in compartments adjacent to lysosomes before merging with pepstatin-positive lysosomes (Fig. 6*B*, *bottom*). Thus, acquisition of enzyme activity and proper targeting to lysosomes in a classical pathway appears to occur only when diffusion in the millisecond range and slow but full exchange in the ER are allowed during maturation in the ER.

DISCUSSION

The dynamics of proteins in living cells are regulated at various levels. Folding depends on the molecules' "breathing," that is, on fluctuations in the relative positions of amino acid residues, but excessive collisions may lead to nonproductive interactions. We therefore reasoned that diffusion should be regulated upon maturation. To examine this process in living cells, it is necessary to manipulate the status of folding. The ts045 strain of VSVG (47) was the only well characterized cargo

[2] A. Kamada, H. Nagaya, T. Tamura, M. Kinjo, H.-Y. Jin, T. Yamashita, K. Jimbow, H. Kanoh, and I. Wada, unpublished data.

available for this purpose. In this paper, we took advantage of the thermal sensitivity of tyrosinase to explore the possibility that tyrosinase folding can be manipulated. We initially examined various naturally occurring temperature-sensitive tyrosinase mutants such as R402Q, P406L, and R422Q (30). However, their thermally induced misfolding was not very reversible and therefore not suitable for experiments to study maturation.[2] However, the folding of wild type tyrosinase was dependent on the incubation temperature, as we were able to show using DOPA oxidase activity as a folding marker (Fig. 1*A*). Although incubation at the permissive temperature did not resolve the structure to the completely native structure (Fig. 4*A*), the molecule still acquired COPII-dependant exportability from the ER (Figs. 4*C* and 6*A*) as well as full DOPA oxidase activity (Fig. 1*A*). We reasoned that these properties were adequate to study the dynamic properties of a maturing cargo protein in the ER.

At present, the expression of chimeric proteins tagged with a fluorescent protein is the only way to study diffusion in living cells. We noticed that the conventional methods for transiently expressing tyrosinase-YFP using lipophilic compounds generally resulted in massive photobleaching when measured with a FCS setup. As a result, we first determined how expression levels affect photobleaching using a glass bead-loading method (42) (Fig. 1*C*). The relationship suggests that any detectable levels of folded tyrosinase-YFP expression significantly influence diffusion in the ER, but as long as the expression level is below a threshold, random diffusion should be measurable. We estimated that tyrosinase-YFP would not be "saturated" in our setup if the expression level was less than 100 kHz. If we assume that the diameter of folded tyrosinase is smaller than 10 nm and if the fluorescence count per single molecule is higher than 3 kHz, as observed, this estimation seems reasonable because the confocal volume (~0.2 fl), which is estimated to contain fewer than 33 molecules, is far larger than the volume that tyrosinase-YFP occupies. Our first conclusion was that the observed diffusion was markedly suppressed at the non-permissive temperature, as measured with FCS. This is based on the results that thermally misfolded tyrosinase showed extensive photobleaching irrespective of the expression level (Fig. 2*A*). As a result of the limited fluctuation, the autocorrelation function could not be applied to this measurement (Fig. 2*B*, *top panel*, and *C*). It is conceivable that this result was caused by the formation of extremely large aggregates. However, this is unlikely because the apparent molecular size of the thermally misfolded tyrosinase was no larger than that synthesized in the presence of castanospermine (Fig. 4*A*).

We thus conjectured that these data indicate a status where random diffusion is restricted by the cellular machinery. This regulation would presumably help to prevent irreversible misfolding because of large aggregate formation by reducing the chance of collision between proteins with exposed hydrophobic patches on their surfaces, and would thereby function to maintain foldability in stressful conditions. Various responses to stress include suppression of translation, induction of heat-shock proteins, and enhanced degradation of misfolded proteins (48). In general, it is thought that aggregation is prevented by the repeated binding of molecular chaperones. Our conclusion may indicate that there is another cellular mechanism that is used to avoid the formation of aggregates, which are thought to be toxic (49–51). Indeed, thermally misfolded tyrosinase showed no particular cytotoxicity, in that it was possible to obtain COS7 cells stably expressing misfolded tyrosinase by culturing them at 40 °C.[2] This may be partly because of the proposed restriction of random diffusion to prevent the formation of aggregates. The observed slow diffusion could be caused by either a regulated association with the immobile matrix or the association with a matrix whose diffusion is thermally regulated. One candidate for the matrix is the ER chaperone network, which is composed of weakly interacting molecular chaperones and folding enzymes (15, 16). Alternatively, it is possible that cells contain protective structures whose phase or conformation is altered upon heat shock.

Similar restriction of diffusion has been described in several reports. For example, in an analysis of protein transport in the plastid tubules of the tobacco plant, two-photon FCS revealed that spontaneous diffusion of expressed green fluorescent proteins in plastids was ~50 times slower than that in the cytosol (52). Interestingly, they found that the FCS recordings included the presence of ATP-dependent active transport, which alternated with "dim periods" in which only random diffusion was seen. This active transport could function to provide long-range transport in a 50-μm plastid tubule. They suggested that the low diffusion coefficient may be caused by fluid-phase viscosity. Similarly, mitochondrial matrix proteins are thought to have slow diffusion because of steric hindrance because of a very high protein concentration in the compartments (53). Interestingly, the dynamics of proteins in the matrix is rather anomalous. Partikian *et al.* (54) showed that green fluorescent protein expressed in the matrix was as highly mobile as in water, although large enzyme complexes in the matrix were almost immobilized, suggesting that the mitochondrial matrix is organized into a highly viscous peripheral area and a central region with low protein density. Another well known example is the nuclear proteins. Extensive FRAP analysis has revealed that molecules in the nucleus show highly diverse dynamics (reviewed by Refs. 55–59) that most likely depend on their associations with DNA, which is nearly immobile on a time scale of several minutes (60).

We thus think that the regulation of immature tyrosinase mobility occurs on at least two different levels. At present, our preferred model is that the FRAP-detectable diffusion may be a result of the cellular machinery for facilitated diffusion in the ER network. Considering that immature proteins are transported through the narrow hollow tubules of the ER to the punctate COPII-coated sites, and that the diameter of the ER tubules are only a few times larger than those of average mature proteins, it is not surprising that active transport of molecules in the ER is required for efficient maturation. Indeed, our current research indicates that the mobility of certain proteins in the ER is regulated.[3] Further studies on the dynamics of maturing proteins should help to understand why folding is so successful in healthy cells continuously exposed to various types of folding stresses that easily terminate folding *in vitro*.

REFERENCES

1. Matlack, K. E., Misselwitz, B., Plath, K., and Rapoport, T. A. (1999) *Cell* **97,** 553–564
2. Kornfeld, R., and Kornfeld, S. (1985) *Annu. Rev. Biochem.* **54,** 631–664
3. Stevens, F. J., and Argon, Y. (1999) *Semin. Cell Dev. Biol.* **10,** 443–454
4. Ferrari, D. M., and Soling, H. D. (1999) *Biochem. J.* **339,** 1–10
5. Freedman, R. B., Klappa, P., and Ruddock, L. W. (2002) *EMBO Rep.* **3,** 136–140
6. Bose, S., and Freedman, R. B. (1994) *Biochem. J.* **300,** 865–870
7. Fewell, S. W., Travers, K. J., Weissman, J. S., and Brodsky, J. L. (2001) *Annu. Rev. Genet.* **35,** 149–191
8. Benham, A. M., and Braakman, I. (2000) *Crit. Rev. Biochem. Mol. Biol.* **35,** 433–473
9. Lord, J. M., Ceriotti, A., and Roberts, L. M. (2002) *Curr. Biol.* **12,** R182–R184
10. Jarosch, E., Geiss-Friedlander, R., Meusser, B., Walter, J., and Sommer, T. (2002) *Traffic* **3,** 530–536
11. Braakman, I. (2001) *EMBO Rep.* **2,** 666–668
12. Gallione, C. J., and Rose, J. K. (1985) *J. Virol.* **54,** 374–382
13. Doms, R. W., Keller, D. S., Helenius, A., and Balch, W. E. (1987) *J. Cell Biol.*

[3] H. Nagaya, T. Tamura, K. Hatsuzawa, H. Hashimoto, and I. Wada, manuscript in preparation.

105, 1957–1969
14. Hammond, C., and Helenius, A. (1994) *J. Cell Biol.* **126,** 41–52
15. Tatu, U., and Helenius, A. (1997) *J. Cell Biol.* **136,** 555–565
16. Meunier, L., Usherwood, Y. K., Chung, K. T., and Hendershot, L. M. (2002) *Mol. Biol. Cell* **13,** 4456–4469
17. Axelrod, D., Koppel, D. E., Schlessinger, J., Elson, E., and Webb, W. W. (1976) *Biophys. J.* **16,** 1055–1069
18. Nehls, S., Snapp, E. L., Cole, N. B., Zaal, K. J., Kenworthy, A. K., Roberts, T. H., Ellenberg, J., Presley, J. F., Siggia, E., and Lippincott-Schwartz, J. (2000) *Nat. Cell Biol.* **2,** 288–295
19. Hendershot, L. M. (2000) *Nat. Cell Biol.* **2,** E105–E106
20. Rigler, R., and Elson, E. L. (2001) *Fluorescence Correlation Spectroscopy: Theory and Applications*, Springer-Verlag, Berlin
21. Elson, E. L. (2001) *Traffic* **2,** 789–796
22. Hess, S. T., Huang, S., Heikal, A. A., and Webb, W. W. (2002) *Biochemistry* **41,** 697–705
23. Widengren, J., and Rigler, R. (1998) *Cell. Mol. Biol. (Noisy-le-grand)* **44,** 857–879
24. Foldes-Papp, Z., Demel, U., and Tilz, G. P. (2001) *Proc. Natl. Acad. Sci. U. S. A.* **98,** 11509–11514
25. Larson, D. R., Ma, Y. M., Vogt, V. M., and Webb, W. W. (2003) *J. Cell Biol.* **162,** 1233–1244
26. Terada, S., Kinjo, M., and Hirokawa, N. (2000) *Cell* **103,** 141–155
27. Hearing, V. J. (1987) *Methods Enzymol.* **142,** 154–165
28. Spritz, R. A., and Hearing, V. J. (1994) in *Advances in Human Genetics* (Hirschhorn, K., and Harris, H., eds) pp. 1–5, Plenum Press, New York
29. Halaban, R., Svedine, S., Cheng, E., Smicun, Y., Aron, R., and Hebert, D. N. (2000) *Proc. Natl. Acad. Sci. U. S. A.* **97,** 5889–5894
30. Toyofuku, K., Wada, I., Spritz, R. A., and Hearing, V. J. (2001) *Biochem. J.* **355,** 259–269
31. Berson, J. F., Frank, D. W., Calvo, P. A., Bieler, B. M., and Marks, M. S. (2000) *J. Biol. Chem.* **275,** 12281–12289
32. Petrescu, S. M., Petrescu, A. J., Titu, H. N., Dwek, R. A., and Platt, F. M. (1997) *J. Biol. Chem.* **272,** 15796–15803
33. Halaban, R., Cheng, E., Zhang, Y., Moellmann, G., Hanlon, D., Michalak, M., Setaluri, V., and Hebert, D. N. (1997) *Proc. Natl. Acad. Sci. U. S. A.* **94,** 6210–6215
34. Branza-Nichita, N., Petrescu, A. J., Dwek, R. A., Wormald, M. R., Platt, F. M., and Petrescu, S. M. (1999) *Biochem. Biophys. Res. Commun.* **261,** 720–725
35. Toyofuku, K., Wada, I., Hirosaki, K., Park, J. S., Hori, Y., and Jimbow, K. (1999) *J. Biochem. (Tokyo)* **125,** 82–89
36. Honing, S., Sandoval, I. V., and von Figura, K. (1998) *EMBO J.* **17,** 1304–1314
37. Simmen, T., Schmidt, A., Hunziker, W., and Beermann, F. (1999) *J. Cell Sci.* **112,** 45–53
38. Calvo, P. A., Frank, D. W., Bieler, B. M., Berson, J. F., and Marks, M. S. (1999) *J. Biol. Chem.* **274,** 12780–12789
39. Setaluri, V. (2000) *Pigment Cell Res.* **13,** 128–134
40. Jimbow, K., Park, J. S., Kato, F., Hirosaki, K., Toyofuku, K., Hua, C., and Yamashita, T. (2000) *Pigment Cell Res.* **13,** 222–229
41. Hirosaki, K., Yamashita, T., Wada, I., Jin, H. Y., and Jimbow, K. (2002) *J. Investig. Dermatol.* **119,** 475–480
42. Nagaya, H., Wada, I., Jia, Y.-J., and Kanoh, H. (2002) *Mol. Biol. Cell* **13,** 302–316
43. Akagi, T., Shishido, T., Murata, K., and Hanafusa, H. (2000) *Proc. Natl. Acad. Sci. U. S. A.* **97,** 7290–7295
44. Spector, D. L., Goldman, R. D., and Leinwand, L. A. (1997) *Cells: A Laboratory Manual*, Vol. 2, Cold Spring Harbor Laboratory Press, Cold Spring Harbor, NY
45. Misumi, Y., Miki, K., Takatsuki, A., Tamura, G., and Ikehara, Y. (1986) *J. Biol. Chem.* **261,** 11398–11403
46. Swaminathan, R., Hoang, C. P., and Verkman, A. S. (1997) *Biophys. J.* **72,** 1900–1907
47. Rose, J. K., and Gallione, C. J. (1981) *J. Virol.* **39,** 519–528
48. Mori, K. (2003) *Traffic* **4,** 519–528
49. Bence, N. F., Sampat, R. M., and Kopito, R. R. (2001) *Science* **292,** 1552–1555
50. Bucciantini, M., Giannoni, E., Chiti, F., Baroni, F., Formigli, L., Zurdo, J., Taddei, N., Ramponi, G., Dobson, C. M., and Stefani, M. (2002) *Nature* **416,** 507–511
51. Dobson, C. M. (2003) *Nature* **426,** 884–890
52. Kohler, R. H., Schwille, P., Webb, W. W., and Hanson, M. R. (2000) *J. Cell Sci.* **113,** 3921–3930
53. Welch, G. R., and Easterby, J. S. (1994) *Trends Biochem. Sci.* **19,** 193–197
54. Partikian, A., Olveczky, B., Swaminathan, R., Li, Y., and Verkman, A. S. (1998) *J. Cell Biol.* **140,** 821–829
55. Misteli, T. (2001) *Science* **291,** 843–847
56. Misteli, T. (2001) *J. Cell Biol.* **155,** 181–185
57. Phair, R. D., and Misteli, T. (2001) *Nat. Rev. Mol. Cell. Biol.* **2,** 898–907
58. Festenstein, R., Pagakis, S. N., Hiragami, K., Lyon, D., Verreault, A., Sekkali, B., and Kioussis, D. (2003) *Science* **299,** 719–721
59. Cheutin, T., McNairn, A. J., Jenuwein, T., Gilbert, D. M., Singh, P. B., and Misteli, T. (2003) *Science* **299,** 721–725
60. Lukacs, G. L., Haggie, P., Seksek, O., Lechardeur, D., Freedman, N., and Verkman, A. S. (2000) *J. Biol. Chem.* **275,** 1625–1629

Available online at www.sciencedirect.com
SCIENCE DIRECT®
Biochemical and Biophysical Research Communications 324 (2004) 849–854
BBRC
www.elsevier.com/locate/ybbrc

Direct detection of caspase-3 activation in single live cells by cross-correlation analysis☆

Kenta Saito[a], Ikuo Wada[b], Mamoru Tamura[a], Masataka Kinjo[a,*]

[a] *Laboratory of Supramolecular Biophysics, Research Institute for Electronic Science, Hokkaido University, N12W6, Kita-ku, Sapporo 060-0812, Japan*
[b] *Department of Cell Science, Institute of Biomedical Sciences, Fukushima Medical University, 1-Banchi, Hikarigaoka, Fukushima 960-1295, Japan*

Received 14 September 2004

Abstract

Dual color fluorescence cross-correlation spectroscopy (FCCS) provides information about the coincidence of spectrally well-defined two fluorescent molecules in a small observation area at the single-molecule level. To evaluate the activity of caspase-3 in vivo directly, FCCS was applied to single live cells. We constructed chimeric proteins that consisted of tandemly fused enhanced green FP (EGFP) and monomeric red FP (mRFP). In control experiments, the protease reaction was monitored in solution, where a decrease in cross-correlation amplitude was observed due to specific cleavage of the amino acid sequence between EGFP and mRFP. Moreover, a decrease in cross-correlation amplitude could be detected in a live cell, where caspase-3 activation was induced by apoptosis. This is the first report of FP-based in vivo cross-correlation analysis. FP-based FCCS may become the most versatile method for analysis of protein–protein interactions in live cells.

Keywords: Fluorescence cross-correlation spectroscopy; Green fluorescent protein; Monomeric red fluorescent protein; Apoptosis-induced protease activation

The fluorescence resonance energy transfer (FRET) technique has been used for studying protein–protein interactions in live cells [1]. However, because FRET efficiency strongly depends on the distance between donor and acceptor fluorophores (~10 nm) even in their appropriate angle, the sizes of the target molecule, and/or interaction molecule are greatly limited.

Instead, fluorescence correlation spectroscopy (FCS) [2] can be applied for this purpose, as it provides information about the mobility of fluorescently tagged target molecules at a very low concentration (~pM) in vitro [3,4] and in vivo [5–8]. FCS measurement is based on single photon counting at the single-molecule level in a defined detection volume (~0.25 fl) generated by an excitation laser beam and fine detection optics. The diffusion constant and the concentration of target molecules can be determined from the auto-correlation function ($G(\tau)$), allowing us to monitor their interactions in situ [3,4,8].

An extended technique of FCS, dual color fluorescence cross-correlation spectroscopy (FCCS), can detect the coincidence of two spectrally distinct fluorescent probes in a small detection area at very low concentrations [9–11]. In principle, this technique is free from the limitations of FRET. FCCS has been used to detect the association–dissociation reaction and interaction between two molecular species in vitro [12–15]. Only a very few attempts have so far been made at the cross-correlation analysis of live cells [16,17]. Herein, we will report the usefulness of fluorescent protein (FP)-based cross-correlation analysis of live cells. For the quantitative

☆ *Abbreviations:* FRET, fluorescence resonance energy transfer; FCS, fluorescence correlation spectroscopy; FCCS, fluorescence cross-correlation spectroscopy; FP, fluorescent protein; EGFP, enhanced green FP; mRFP, monomeric red FP.

* Corresponding author. Fax: +81 11 706 4964.
E-mail address: kinjo@imd.es.hokudai.ac.jp (M. Kinjo).

0006-291X/$ - see front matter © 2004 Elsevier Inc. All rights reserved.
doi:10.1016/j.bbrc.2004.09.126

evaluation of cross-correlation, we constructed a chimeric protein in which enhanced green FP (EGFP) is fused to monomeric red FP (mRFP) [18] via two types of 29 linker sequences cleaved by either enterokinase [19] or caspase-3 [20]. For the first time, we report here that caspase-3 reaction can be detected in vitro and in vivo through the decrease of cross-correlation amplitude due to protease cleavage of a specific recognition sequence between EGFP and mRFP.

Experimental procedures

Cell preparation. HeLa cells were grown in a 5% CO_2 humidified atmosphere at 37 °C in Dulbecco's modified Eagle's medium (DMEM) supplemented with 10% fetal bovine serum, 2×10^5 U/L penicillin G, and 200 mg/L streptomycin sulfate. Transfection of HeLa cells grown on LAB-TEK chambered coverslips with eight wells (Nalge Nunc International) was performed using FuGENE 6 (Roche Molecular Biochemicals). During FCCS measurements, HeLa cells were maintained in Opti-MEM I reduced-serum medium (Invitrogen).

Plasmid construction. Enterokinase (ek) or caspase-3 (c3) recognition sites were engineered in the N-terminus of mRFP (R) or tandem mRFP dimer (R_2) by polymerase chain reaction (PCR). The PCR products were digested and ligated into the multiple cloning site of pEGFP-C1 (Clontech). These plasmids encode EGFP (G) and R or R_2 fusion proteins (EGFP-mRFP chimera), G-X-R and G-X-R_2, in which X = D_4K in the case of enterokinase recognition site, X = DEVD in the case of caspase-3 recognition site.

Protease assay. Proteins (G, R, R_2, G-X-R, and G-X-R_2) for in vitro measurements were produced using a wheat germ extract (cell-free) translation system [21]. First, 10.0 μl of EGFP-mRFP chimera was incubated with 0.016 U/μl of recombinant enterokinase (Novagen) at room temperature. The enterokinase reaction mixture contained 20 mM Tris–HCl, pH 7.4, 50 mM NaCl, and 2 mM $CaCl_2$. Then 10.0 μl of EGFP-mRFP chimera was incubated with 1.0 U/μl caspase-3 (Calbiochem) at 37 °C. The caspase-3 reaction mixture contained 20 mM Hepes–KOH, pH 7.4, 10 mM KCl, 1.5 mM $MgCl_2$, 1 mM EDTA, 1 mM EGTA, and 10 mM DTT. For in vivo protease reaction assay, HeLa cells were treated with 50 ng/ml tumor necrosis factor-α (TNF-α) and 10 μg/ml cycloheximide (CHX).

Microscopy. Live cell fluorescence imaging was performed using an inverted confocal laser scanning microscope LSM510 (Carl Zeiss). EGFP was excited at the 488 nm laser line of a CW Ar^+ laser and mRFP was excited at the 543 nm laser line of a CW He–Ne laser through a water immersion objective (C-Apochromat, 40×, 1.2NA; Carl Zeiss). Emission signals were detected at 505–550 nm for EGFP and >560 nm for mRFP by sequential scanning.

FCCS measurement. FCCS measurements were carried out mainly with a ConfoCor2 (Carl Zeiss), which consisted of a CW Ar^+ laser and He–Ne laser, a water immersion objective (C-Apochromat, 40×, 1.2NA; Carl Zeiss), and two channels of avalanche photodiodes (SPCM-200-PQ; EG&G). The confocal pinhole diameter was adjusted to 90 μm. EGFP was excited at the 488 nm laser line and mRFP was excited at the 543 nm laser line. The emission signals were split by a dichroic mirror (570 nm beam splitter) and detected at 505–530 nm by the green channel for EGFP and at 600–650 nm by the red channel for mRFP. FCCS measurements were also carried out with a Leica FCS system (Leica). In this system, EGFP was excited at the 488 nm laser line and mRFP was excited at the 594 nm laser line. Emission signals were detected at 505–530 nm for EGFP and 607–683 nm for mRFP.

Data analysis. The fluorescence auto-correlation functions of the red and green channels, $G_r(\tau)$ and $G_g(\tau)$, and the fluorescence cross-correlation function, $G_c(\tau)$, are calculated by

$$G_x(\tau) = \frac{\langle \delta I_i(t) \cdot \delta I_i(t+\tau) \rangle}{\langle I_i(t) \rangle \langle I_j(t) \rangle}, \tag{1}$$

where τ denotes the time delay, I_i is the fluorescence intensity of the red channel (i = r) or green channel (i = g), $G_r(\tau)$, $G_g(\tau)$, and $G_c(\tau)$ denote the auto-correlation functions of red ($i = j = x$ = r), green ($i = j = x$ = g), and cross (i = r, j = g, and x = c), respectively. Acquired $G(\tau)$ were fitted by a one-, two-, or three-component model as

$$G(\tau) = \frac{1}{N} \sum_i F_i \left(1 + \frac{\tau}{\tau_i}\right)^{-1} \left(1 + \frac{\tau}{s^2 \tau_i}\right)^{-1/2}. \tag{2}$$

where F_i and τ_i are the fraction and diffusion time of component i, respectively. N is the average number of fluorescent particles in the excitation-detection volume defined by radius w_0 and length $2z_0$, and s is the structure parameter representing the ratio $s = z_0/w_0$. The average numbers of red fluorescent particles (N_r), green fluorescent particles (N_g), and particles that have both red and green fluorescence (N_c) can be calculated by

$$N_r = \frac{1}{G_r(0)}, \quad N_g = \frac{1}{G_g(0)}, \quad \text{and } N_c = \frac{G_c(0)}{G_r(0) \cdot G_g(0)}, \tag{3}$$

respectively. When N_r and N_g are constant, $G_c(0)$ is directly proportional to N_c. For quantitative evaluation of cross-correlation among various samples, $G_c(0)$ is normalized by $G_g(0)$ (relative cross-correlation amplitude; $G_c(0)/G_g(0)$).

Results

In vitro control experiments

To assess the degree of cross-correlation ($G_c(\tau)$); see experimental procedures quantitatively, FCCS measurements were carried out with purified proteins in PBS. Since the brightness of mRFP is very weak [18], to improve it, we also constructed another probe in which additional mRFP coding sequence was inserted after an EGFP-mRFP chimera (EGFP fused to tandem mRFP dimer). Fluorescent intensity at the red channel of the G-DEVD-R_2 was about 2-fold that of G-DEVD-R (Figs. 1A and C, insets). A mixture of EGFP and mRFP, which are referred to as MixGR and MixGR_2, were used as control samples against the linked proteins, G-DEVD-R and G-DEVD-R_2. The concentrations of the mixture of EGFP and mRFP, MixGR, and MixGR_2 were prepared to have the roughly the same green and red fluorescent intensity ratios as the EGFP-mRFP chimera (Figs. 1A–D, insets). Amplitudes of auto-correlation curves were almost the same for G-DEVD-R and MixGR (Figs. 1A and B), and for G-DEVD-R_2 and MixGR_2 (Figs. 1C and D). In contrast, amplitudes of cross-correlation were only apparent in G-DEVD-R and G-DEVD-R_2 (Figs. 1A and C) but almost absent in a mixture of EGFP and mRFP (Figs. 1B and D). We considered that the small value $G_c(0)/G_g(0)$ of the mixture of EGFP and mRFP (Table 1) was the background due to the leakage of EGFP emission through the red channel detector (red detector cross-talk) because $G_c(0)/G_g(0)$ of mixture of EGFP and mRFP became larger at a higher EGFP